the induction of proinflammatory cytokines (interleukin (IL)-6, tumor necrosis factor-α, and IL-10) and cyclooxygenase-2. Polyplexes with B/H = 0/100 formulation induced significantly higher mRNA levels of these inflammation-related molecules compared with other formulations 4 hours after administration (Figure 3). The other PEGylated polyplexes (B/H = 100/0 and 50/50) induced much lower expressions of these molecules than polyplexes with B/H = 0/100 formulation, although the levels of these molecules in the PEGylated groups were slightly higher compared with the control groups that received naked pDNA or buffer.

Furthermore, we evaluated the inflammatory responses to administration of identical amounts of free polymers (B or H) that were used to form the polyplexes of B/H = 100/0 or 0/100 formulations, respectively. The free polymers induced inflammatory responses that were similarly low to those by PEGylated polyplexes (B/H = 100/0 and 50/50) (**Figure 3**). Thus, it is suggested that the complexation of H polymer with pDNA augmented the inflammatory responses in the lungs compared with the state of free H polymer. In contrast, PEG effectively shielded the polyplexes and reduced the inflammatory responses in the lungs.

After 24 hours of administration, cytokine inductions were similar to the levels observed in the controls (**Supplementary Figure S1**), suggesting that the inflammation was transient and the PAsp(DET) polycation induced no persistent tissue damage, presumably because of the biodegradability of PAsp(DET).[17] In blood tests conducted 24 hours after administration, there were no significant changes in the cell counts of white and red blood cells, and the items for evaluations of liver and kidney functions, and C-reactive protein, a sensitive marker for inflammatory responses, remained in an undetectable level (**Supplementary Figure S2**).

Regulation of inflammatory responses in the lungs by PEG shielding

Histopathological analyses were performed to investigate the mechanisms between transfection capacity and toxicity. An increase in the infiltration of inflammatory cells was observed 4 hours after administration of polyplexes with B/H = 0/100 formulations (**Figure 4c**). In contrast, following administration of the PEGylated polyplexes (B/H = 100/0 and 50/50), the alveolar structures remained intact without infiltration of inflammatory cells (**Figure 4a,b**), showing good correlations with the results of proinflammatory cytokine inductions (**Figure 3**).

To determine the mechanisms underlying the inflammatory responses, we observed the uptake of polyplexes by macrophages. Cy5-labeled pDNAs were introduced into the lungs, followed by immunostaining using an F4/80 antibody for macrophages and Hoechst 33342 for cell nuclei. On obtaining fluorescent microscopic images, we quantified the fluorescence intensities of pDNAs that were colocalized in the macrophages, using an image-analysis software (In Cell Analyzer 1000 Workstation ver.3.5; GE Healthcare UK, Buckinghamshire, UK). Representative microscopic images are shown in Figure 5a–d. As observed in the histograms of the pDNA intensity in each macrophage (Figure 5e),

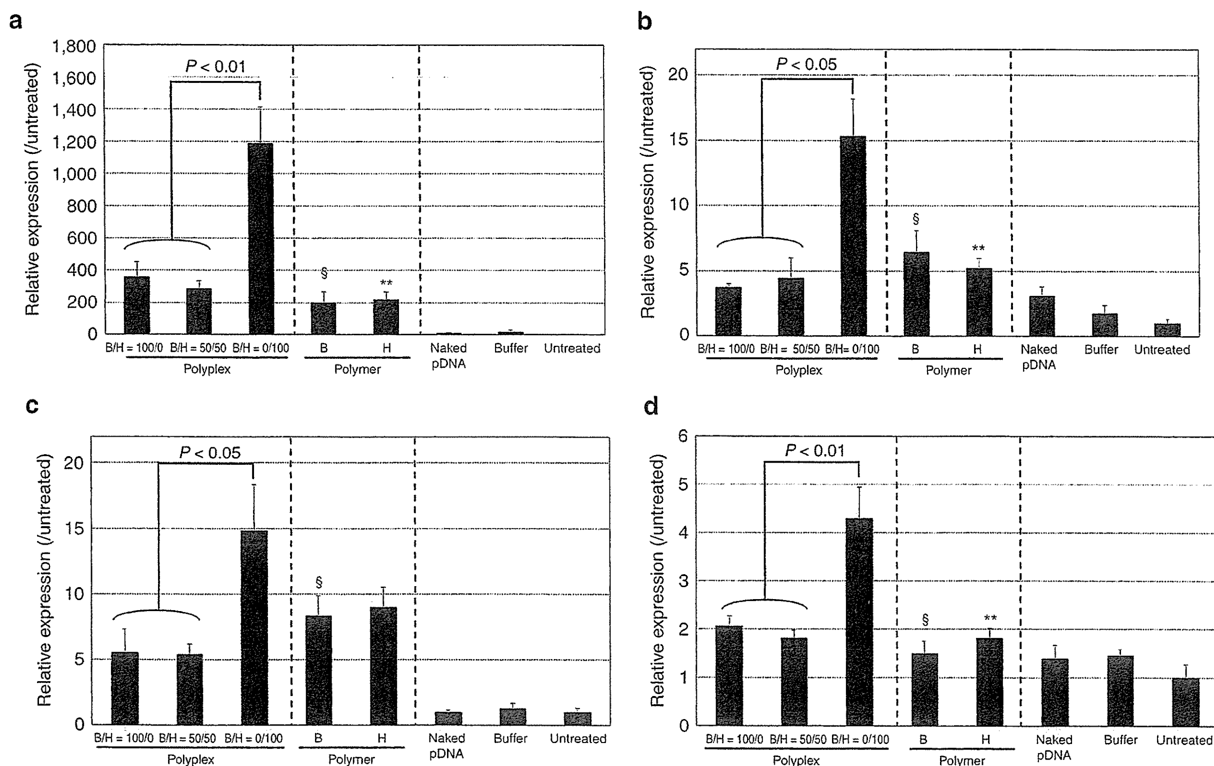

Figure 3 Messenger RNA expression of cytokines (a) interleukin (IL)-6, (b) tumor necrosis factor-α (TNF-α), (c) IL-10, and (d) cyclooxygenase-2 (Cox-2) in lung tissue 4 hours after administration of polyplexes, identical amount of free polymers, plasmid DNAs (pDNAs), or buffer. The data were expressed as the means ± SEM (*N* = 5). §Nonsignificance versus polyplexes with B/H = 100/0 formulation, $^{**}P < 0.01$ versus polyplexes with B/H = 0/100 formulation.

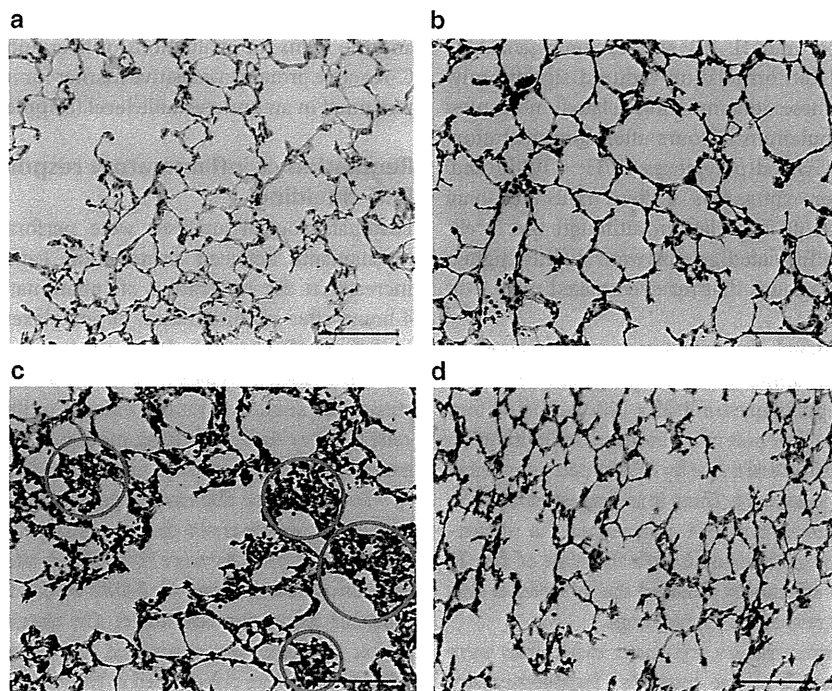

Figure 4 Histological analyses of lung in hematoxylin and eosin stained sections. The images were taken 4 hours after administration of polyplexes with (**a**) B/H = 100/0, (**b**) B/H = 50/50, or (**c**) B/H = 0/100 formulation. (**d**) Control was not administered polyplexes. Bars = 100 μm. In (**c**), representative infiltration of inflammatory cells is marked by red circles.

polyplexes with B/H = 0/100 formulation were taken up by the macrophages to a significantly higher extent compared with the PEGylated polyplexes (B/H = 100/0 and 50/50).

Macrophages are known to effectively ingest large particles (≥500 μm) by phagocytosis.[28] Thus, it is assumed that aggregation of polyplexes in lung tissue may significantly affect the activity of macrophages. Analysis of aggregation of polyplexes under conditions mimicking that observed in the lungs was performed. We observed polyplexes-containing Cy5-labeled pDNAs in the presence of bronchoalveolar lavage fluid (BALF) obtained from mice. Fluorescence microscopy showed a clear contrast between the polyplexes depending on the proportion of H; PEGylated polyplexes (B/H = 100/0 and 50/50) showed uniformly distributed Cy-5 signals during BALF incubation for up to 90 minutes (Figure 6). In contrast, polyplexes with 0/100 formulation showed large spots of Cy-5 signals after 30 minutes of BALF incubation. Thus, it is likely that particle aggregation of B/H = 0/100 formulation was promptly induced under the physiological circumstances in the lungs. Based on the obvious relationship between these findings and the cytokine induction data (Figure 3), we suggest that the aggregation of polyplexes with B/H = 0/100 formulation activated macrophages to rapidly ingest these polyplexes.

Enhancement of transgene expressions in the presence of H polycations

Increased proportions of H enhanced *in vitro* transgene expression (Figure 1). We have already revealed that PAsp(DET) has an excellent capacity of endosomal escape because of acidity-induced membrane destabilization.[16] For the analylsis, an enzymatic assay to detect leakage of cytoplasmic enzyme (lactate dehydrogenase) was done after addition of free polycations to culture cells. However, this experiment has difficulty in detecting the initial changes within several ten minutes after transfection.

In the present study, we used a novel method that allows the evaluation of cell membrane integrity in a highly sensitive manner using a nuclear-binding fluorescence molecule such as YO-PRO1 or ethidium bromide.[29,30] After transfection using polyplexes from B/H formulations, the cells were treated with YO-PRO1 because YO-PRO1, which was impermeable to the normal cell membrane, can penetrate membranes of cells with perturbed integrity and emit a strong fluorescent signal due to DNA intercalation.[31] As shown in **Figure 7**, after 30 minutes of transfection under acidic conditions, polyplexes with B/H = 50/50 formulation destabilized cell membranes to a similar level as polyplexes with B/H = 0/100 formulation, whereas polyplexes with B/H = 100/0 formulation, similar to untreated control, did not destabilize membranes even at pH 5.5. Thus, it can be said that presence of H polycations caused efficient endosomal escape of polyplexes shortly after transfection.

Following *in vivo* administration to the lungs, we evaluated the amount of pDNA that was taken up into the lung tissues by collecting total DNA, followed by quantitative PCR analyses using specific primers for the pDNA. Prior to the extracting lung tissue, extensive bronchoalveolar lavage (BAL) was done to remove pDNAs existing in the extracellular space. Interestingly, 24 hours after introduction of pDNA into the lungs, the amount of pDNA did not show any significant difference among polyplexes formed by different B/H formulations (**Supplementary Figure S3**). Therefore, it is reasonably assumed that the differences in transgene expressions in the lungs (Figure 2) are not attributable to

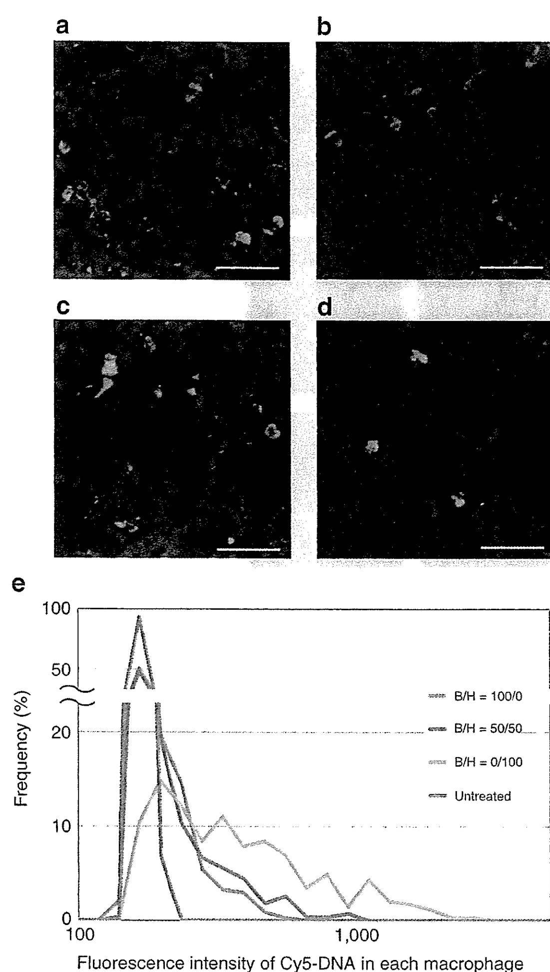

Figure 5 Uptake of polyplexes by macrophages in lung. Fluorescent microscopic images were taken at 4 hours after polyplex administration. The polyplexes were prepared using Cy-5 labeled plasmid DNA (pDNA) (red). The macrophages were immunostained using anti-F4/80 antibodies (green). The cell nuclei were stained with Hoechst 33342 (blue). Representative images of polyplexes with (**a**) B/H = 100/0, (**b**) B/H = 50/50, (**c**) B/H = 0/100 formulations, or (**d**) control tissue without gene administration. Bars = 50 µm. (**e**) Quantification of the amount of pDNA colocalizing in each macrophage. The fluorescence intensities of Cy-5 labeled pDNA in each macrophage were quantified using an image-analyzing software, and displayed as a histogram representing the pDNA intensity in each macrophage.

the uptake of polyplexes into cells, but to the capacities of H polycations to facilitate intracellular processes of endosomal escape, although the direct observation of intracellular behavior of polyplexes was difficult *in vivo*.

DISCUSSION

Inflammation is a key factor in nanoparticle toxicity.[6,11,32] This is a rapid process that is initially triggered by antioxidant responses within a few hours of exposure of biological tissue to nanoparticles. Thus, it is important to evaluate these responses shortly after the administration of nanoparticles.

In the present study, we determined that PEG shielding of pDNA-containing nanoparticles reduces inflammatory responses in the lungs. PEGylated polyplexes (B/H = 100/0 and 50/50) effectively alleviated inflammatory responses compared with polyplexes with B/H = 0/100 formulation. Since the administration of free cationic polymers into the lungs did not induce such inflammatory responses, we assume that the cationic nature of polyplexes was not the only cause of these responses. Otherwise, the aggregation behavior was different among polyplexes. Polyplexes with B/H = 0/100 formulation showed rapid aggregation in BALF, whereas PEGylated polyplexes (B/H = 100/0 and 50/50) did not aggregate even after incubation for > 90 minutes (Figure 6). These observations are clearly concordant with the tendency to induce cytokine expression and polyplex uptake by macrophages in the lungs (Figure 3). Thus, it is reasonable to assume that aggregation of polyplex with B/H = 0/100 formulation in lung tissue caused a high uptake of the polyplexes by macrophages, which led to strong inflammatory responses and the decreased transgene expressions in the lung.

Conversely, the presence of PEG on the surface of polyplexes effectively prevents inflammatory responses. Although PEG effectively prevented aggregation, *in vitro* and *in vivo* transgene expressions were compromised by the increase in B polycation. Since pDNA amounts in lung tissues after introduction of polyplexes were not different among the B/H formulations (**Supplementary Figure S3**), the decrease in the transgene expressions in parallel with the increased ratios of PEG, appeared to be chiefly due to the effects of PEG to hamper the intracellular processes of polyplexes. Membrane destabilization at pH 5.5 was enhanced by the increased amounts of H polycations (Figure 7), suggesting a critical role for H polycations without PEG in facilitating the endosomal escape of polyplexes.[33] As a consequence, polyplexes with B/H = 50/50 formulation showed the highest transgene expression levels with minimal inflammatory responses in the lungs. This formulation successfully took advantage of both effective PEG shielding and the functioning of PAsp(DET) polycations to enhance intracellular processes.

These observations highlight the importance of analyzing intravital behavior of polyplexes from the standpoint of nanotoxicology. Typically presented as transgene expressions in this study, therapeutic outcomes with nanoscale polyplexes can be easily influenced by slight structural modifications, even when no appreciable changes are detected in their *in vitro* physicochemical evaluations. Careful consideration of all processes from polyplex formation to the intravital behavior is required for effective and safe gene and drug delivery systems, especially for administration to the respiratory system.

Based on our originally developed polycation PAsp(DET), which possesses high endosomal escaping capability with minimal toxicity due to its biodegradable nature, we determined the optimal composition of polyplexes for intratracheal administration of pDNA by tuning the mixing ratio of PEG-block-PAsp(DET) (B) and homo PAsp(DET) (H). *In vitro* transgene expressions increased in parallel with increased proportions of H. In contrast, following *in vivo* intratracheal administration into the lungs, polyplexes with B/H = 0/100 formulation significantly induced proinflammatory cytokines and cyclooxygenase-2 expressions, and resulted in histological findings characteristic of inflammation. Using fluorescence microscopy, we found that BALF containing the polyplexes with B/H = 0/100 formulations exhibited rapid aggregate formation. It is thus reasonable to assume that the rapid aggregation of polyplexes with

© The American Society of Gene & Cell Therapy

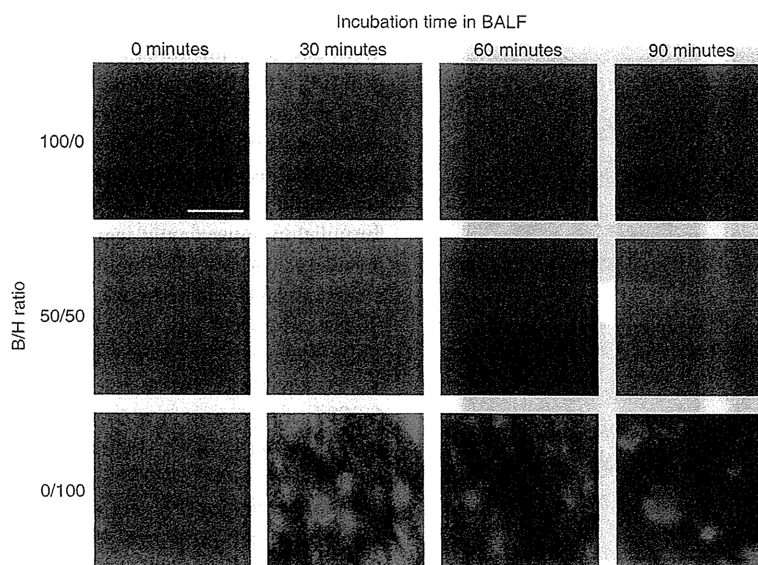

Figure 6 Aggregation of polyplexes during the incubation in bronchoalveolar lavage fluid (BALF). The polypexes were prepared from Cy5-labeled plasmid DNAs (pDNAs), and after adding BALF, the polyplex solutions were observed by a fluorescent microscope. Bar = 50 μm.

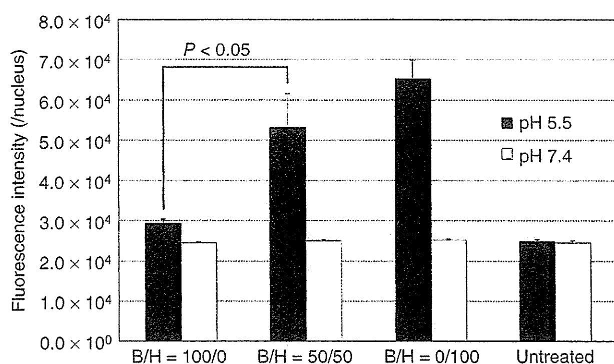

Figure 7 Evaluation of cell membrane destabilization at pH 5.5 or 7.4 in the culture medium. After 30 minutes of transfection toward HuH-7, cells were treated with YO-PRO1. The fluorescence intensity in each cell nucleus, indicating the amount of YO-PRO1 penetration through the plasma membrane, was determined using IN Cell Analyzer 1000. The averages from about 3,000 cells were analyzed in each well. The data were expressed as the means ± SEM ($N = 5$).

B/H = 0/100 formulation in the lung may elicit acute inflammatory responses, resulting in reduced transgene expressions. Notably, appropriate PEG shielding of the polyplex prevented aggregate formation effectively, and polyplexes with B/H = 50/50 formulation achieved appreciable gene expression in the lungs without inflammatory responses. Therefore, this polyplex formulation is a highly practical system for gene therapy for the respiratory system that takes advantage of both effective PEG shielding and functioning of PAsp(DET) polycations to enhance endosomal escape.

MATERIALS AND METHODS

Materials. PEG-block-PAsp(DET) block copolymer (B) and PAsp(DET) homo polymer (H) were synthesized as previously reported.[13] The PEG used in this study had a molecular weight of 12,000 Da. The degree of polymerization of PAsp(DET) portion for B and H was determined by ^{1}H-NMR analyses to be 60 and 55, respectively. CpG-depleted pDNA encoding luciferase (pCpG-ΔLuc) was kindly provided by Makiya Nishikawa from Kyoto University (Kyoto, Japan), which had been constructed as previously reported.[34] The pDNA was amplified in GT115 Escherichia coli (InvivoGen, San Diego, CA) and purified using NucleoBond Xtra EF (Nippon Genetics, Tokyo, Japan). The pDNA concentration was determined spectroscopically at 260 nm. Dulbecco's modified Eagle's medium and fetal bovine serum were purchased from Sigma–Aldrich (St Louis, MO) and Life Technologies Japan (Tokyo, Japan), respectively. Linear polyethylenimine (Exgen 500, molecular weight = 22 kDa) was purchased from MBI FerMentas (Burlington, Ontario, Canada).

Preparation of polyplex solutions. Each polyplex sample was prepared by mixing pDNA and polycations B and/or H at the indicated ratio. The N/P ratio [(total amines in polycations)]/(DNA phosphates)] was fixed at eight throughout the study.

In vitro transfection. Mouse embryonic fibroblast and hepatocellular carcinoma (HuH-7) cells were seeded at a density of 5,000 cells/well in 96-well culture plates and incubated overnight in 100 ml Dulbecco's modified Eagle's medium supplemented with 10% fetal bovine serum and penicillin/streptomycin. For each transfection, the culture medium was replaced with fresh medium containing 10% fetal bovine serum, and the polyplex solution containing 0.25 μg of pDNA was administered to each well. Luciferase expression was measured with the Luciferase assay system (Promega, Madison, WI) and the GloMaxTM 96 microplate luminometer (Promega) according to the manufacturer's protocol.

Intratracheal gene introduction into mouse lungs. BALB/c mice (female, 7 weeks old) were purchased from Charles River Laboratories (Yokohama, Japan). Mice were anesthetized intraperitoneally with pentobarbital (60 mg/kg) (Kyoritsu Seiyaku, Tokyo, Japan). Fifty microliter of polyplex solution containing 10 μg pDNA was administered using a microsprayer model IA-1C-R (Penn Century, Philadelphia, PA) after tracheostomies. All animal protocols were conducted with the approval of the Animal Care and Use Committee, University of Tokyo, Tokyo, Japan.

Evaluation of luciferase expressions in lung. Mice were sacrificed after 24 hours, and lung was excised and thoroughly homogenized using a Multibeads shocker (Yasui Kikai, Osaka, Japan). Luciferase expression was

© The American Society of Gene & Cell Therapy

measured by a luciferase assay system using the Lumat LB9507 luminometer (Berthold, Bad Wildbad, Germany). The expression was normalized to protein concentrations in the cell lysates.

Histological evaluations. Lung specimens were fixed in 10% formalin for 24 hours and embedded in paraffin. These sections (5-µm thick) were stained with hematoxylin and eosin. For evaluations of polyplex behavior and macrophages, pDNA was labeled with Cy-5 using Label IT Tracker Intracellular Nucleic Acid Localization Kits (Mirus, Madison, WI) following manufacturer's protocol. Mice were sacrificed after 4 hours and the excised lung tissue was fixed in 10% formalin for 5 hours, followed by overnight incubation in 20% sucrose/phosphate-buffered saline (PBS) solution at room temperature. The specimens were frozen and sectioned at a 10-µm thickness in a cryostat. Macrophages were immunostained with an anti-F4/80 monoclonal antibody (AbD Serotec, Oxford, UK) at a dilution of 1:300 and an Alexa488-conjugated secondary antibody (Invitrogen, Carlsbad, CA). After staining the nuclei with Hoechst 33342 (Dojindo, Kumamoto, Japan), the sections were observed with a fluorescence microscope equipped with image-analysis software (IN Cell Analyzer 1000; GE Healthcare UK), followed by the measurement of fluorescence intensity of Cy-5 labeled DNA in each macrophage. About 300 macrophages were analyzed for each group.

Measurement of proinflammatory cytokines. To measure mRNA levels of proinflammatory cytokines (IL-6, tumor necrosis factor-α, and IL-10) and cyclooxygenase-2, lung tissue was extracted and total RNA was isolated using an RNeasy Mini Preparation Kit (Qiagen, Hilden, Germany) following manufacturer's protocol. Gene expressions were analyzed by real-time quantitative PCR using TaqMan Gene Expression Assays (Mm00446190_m1 for IL-6, Mm00443258 for tumor necrosis factor-α, Mm 01288386_m1 for IL-10, Mm01307334_g1 for cyclooxygenase-2, and Mm00607939 for β-actin) and an ABI Prism 7500 Sequence Detector (Applied Biosystems, Foster City, CA).

Observation of aggregation in BALF. BAL was performed with 500 µl PBS (instilled and recovered four times), and the BAL fluid (BALF) obtained was centrifuged at 300*g*. To observe the aggregation of polyplexes, Cy5-labeled DNA was used to prepare polyplex solutions at DNA concentration of 33.3 µg/ml. BALF was added to equal volumes of polyplex solutions and observed with an Axiovert 200 fluorescence microscope (Carl Zeiss, Jena, Germany) using a 20× EC Plan Neofuar objective (Carl Zeiss).

Measurement of cellular uptake in lung cells. BAL was conducted eight times, using 500 µl PBS in each time, to remove extracellular pDNA. Next, pDNA was collected from the excised lung tissue and purified using a Wizard Genomic DNA Purification Kit (Promega). Purified DNA was then subjected to a real-time PCR to quantify pDNA copies using an ABI Prism 7500 Sequence Detector (Applied Biosystems). The forward primer (TCTGTGGCTTCAGAGTGGTG) and reverse primer (CTGATTCCTGGGAGATGGAA) were used because they are specific for pCpG-ΔLuc. The copy number of β-actin was also determined by TaqMan Gene Expression Assays to normalize the cell number.

Evaluation of endosomal escape inside cells. HuH-7 cells were seeded at a density of 10,000 cells/well in a 48-multiwell plate and cultured for 24 hours. The culture medium was then replaced with PBS buffer (pH 7.4) or MES buffer (pH 5.5) containing 20 mmol/l MES and 150 mmol/l NaCl; a polyplex solution containing 0.5 µg pDNA was added to each well. The cells were treated with 1 µmol/l YO-PRO1 (Invitrogen) and 2.5 µg/ml Hoechst 33342 in PBS 30 minutes later. The fluorescence intensity of each nucleus was quantified after a 10-minute incubation using an IN Cell Analyzer 1000.

SUPPLEMENTARY MATERIAL

Figure S1 . Messenger RNA expression of proinflammatory cytokines and Cox-2 in lung at 4 hours and 24 hours after transfection.
Figure S2. Blood tests at 24 hours after administration.
Figure S3. Uptake of polyplexes by lung cells at 24 hours after transfection.

ACKNOWLEDGMENTS

We deeply appreciate Makiya Nishikawa (Kyoto University) for providing pDNA (pCpG-ΔLuc), and E.S. (National Cerebral and Cardiovascular Center Research Institute) for technical advices on lung administration of polyplexes. This work was financially supported in part by the Core Research Program for Evolutional Science and Technology (CREST) from Japan Science and Technology Corporation (JST) (K.K.), Grants-in-Aid for Scientific Research form the Japanese Ministry of Education, Culture, Sports, Science and Technology, Japan (MEXT) (K.I.), Global COE Program "Medical System Innovation on through Multidisciplinary Integration" from MEXT, Japan, and Funding Program for World-Leading Innovative R&D on Science and Technology (FIRST Program) from the Japan Society for the Promotion of Science (JSPS). We also thank Satomi Ogura, Yoko Hasegawa, and Katsue Morii (The University of Tokyo) for technical assistance.

REFERENCES

1. Howell, TH, Fiorellini, J, Jones, A, Alder, M, Nummikoski, P, Lazaro, M *et al.* (1997). A feasibility study evaluating rhBMP-2/absorbable collagen sponge device for local alveolar ridge preservation or augmentation. *Int J Periodontics Restorative Dent* **17**: 124–139.
2. Sanders, N, Rudolph, C, Braeckmans, K, De Smedt, SC and Demeester, J (2009). Extracellular barriers in respiratory gene therapy. *Adv Drug Deliv Rev* **61**: 115–127.
3. Oupický, D, Konák, C, Ulbrich, K, Wolfert, MA and Seymour, LW (2000). DNA delivery systems based on complexes of DNA with synthetic polycations and their copolymers. *J Control Release* **65**: 149–171.
4. Kakizawa, Y and Kataoka, K (2002). Block copolymer micelles for delivery of gene and related compounds. *Adv Drug Deliv Rev* **54**: 203–222.
5. De Smedt, SC, Demeester, J and Hennink, WE (2000). Cationic polymer based gene delivery systems. *Pharm Res* **17**: 113–126.
6. Nel, A, Xia, T, Mädler, L and Li, N (2006). Toxic potential of materials at the nanolevel. *Science* **311**: 622–627.
7. Card, JW, Zeldin, DC, Bonner, JC and Nestmann, ER (2008). Pulmonary applications and toxicity of engineered nanoparticles. *Am J Physiol Lung Cell Mol Physiol* **295**: L400–L411.
8. Bonner, JC (2010). Nanoparticles as a potential cause of pleural and interstitial lung disease. *Proc Am Thorac Soc* **7**: 138–141.
9. Poland, CA, Duffin, R, Kinloch, I, Maynard, A, Wallace, WA, Seaton, A *et al.* (2008). Carbon nanotubes introduced into the abdominal cavity of mice show asbestos-like pathogenicity in a pilot study. *Nat Nanotechnol* **3**: 423–428.
10. Ryman-Rasmussen, JP, Cesta, MF, Brody, AR, Shipley-Phillips, JK, Everitt, JI, Tewksbury, EW *et al.* (2009). Inhaled carbon nanotubes reach the subpleural tissue in mice. *Nat Nanotechnol* **4**: 747–751.
11. Beyerle, A, Irmler, M, Beckers, J, Kissel, T and Stoeger, T (2010). Toxicity pathway focused gene expression profiling of PEI-based polymers for pulmonary applications. *Mol Pharm* **7**: 727–737.
12. Dailey, LA, Jekel, N, Fink, L, Gessler, T, Schmehl, T, Wittmar, M *et al.* (2006). Investigation of the proinflammatory potential of biodegradable nanoparticle drug delivery systems in the lung. *Toxicol Appl Pharmacol* **215**: 100–108.
13. Kanayama, N, Fukushima, S, Nishiyama, N, Itaka, K, Jang, WD, Miyata, K *et al.* (2006). A PEG-based biocompatible block catiomer with high buffering capacity for the construction of polyplex micelles showing efficient gene transfer toward primary cells. *ChemMedChem* **1**: 439–444.
14. Masago, K, Itaka, K, Nishiyama, N, Chung, UI and Kataoka, K (2007). Gene delivery with biocompatible cationic polymer: pharmacogenomic analysis on cell bioactivity. *Biomaterials* **28**: 5169–5175.
15. Harada-Shiba, M, Takamisawa, I, Miyata, K, Ishii, T, Nishiyama, N, Itaka, K *et al.* (2009). Intratracheal gene transfer of adrenomedullin using polyplex nanomicelles attenuates monocrotaline-induced pulmonary hypertension in rats. *Mol Ther* **17**: 1180–1186.
16. Miyata, K, Oba, M, Nakanishi, M, Fukushima, S, Yamasaki, Y, Koyama, H *et al.* (2008). Polyplexes from poly(aspartamide) bearing 1,2-diaminoethane side chains induce pH-selective, endosomal membrane destabilization with amplified transfection and negligible cytotoxicity. *J Am Chem Soc* **130**: 16287–16294.
17. Itaka, K, Ishii, T, Hasegawa, Y and Kataoka, K (2010). Biodegradable polyamino acid-based polycations as safe and effective gene carrier minimizing cumulative toxicity. *Biomaterials* **31**: 3707–3714.
18. Maruyama, K, Yuda, T, Okamoto, A, Kojima, S, Suginaka, A and Iwatsuru, M (1992). Prolonged circulation time *in vivo* of large unilamellar liposomes composed of distearoyl phosphatidylcholine and cholesterol containing amphipathic poly(ethylene glycol). *Biochim Biophys Acta* **1128**: 44–49.
19. Ogris, M, Brunner, S, Schüller, S, Kircheis, R and Wagner, E (1999). PEGylated DNA/transferrin-PEI complexes: reduced interaction with blood components, extended circulation in blood and potential for systemic gene delivery. *Gene Ther* **6**: 595–605.
20. Verbaan, FJ, Oussoren, C, Snel, CJ, Crommelin, DJ, Hennink, WE and Storm, G (2004). Steric stabilization of poly(2-(dimethylamino)ethyl methacrylate)-based polyplexes mediates prolonged circulation and tumor targeting in mice. *J Gene Med* **6**: 64–75.

© The American Society of Gene & Cell Therapy

21. Itaka, K and Kataoka, K (2009). Recent development of nonviral gene delivery systems with virus-like structures and mechanisms. *Eur J Pharm Biopharm* **71**: 475–483.
22. Kursa, M, Walker, GF, Roessler, V, Ogris, M, Roedl, W, Kircheis, R *et al.* (2003). Novel shielded transferrin-polyethylene glycol-polyethylenimine/DNA complexes for systemic tumor-targeted gene transfer. *Bioconjug Chem* **14**: 222–231.
23. Allen, TM, Mehra, T, Hansen, C and Chin, YC (1992). Stealth liposomes: an improved sustained release system for 1-beta-D-arabinofuranosylcytosine. *Cancer Res* **52**: 2431–2439.
24. Itaka, K, Ohba, S, Miyata, K, Kawaguchi, H, Nakamura, K, Takato, T *et al.* (2007). Bone regeneration by regulated *in vivo* gene transfer using biocompatible polyplex nanomicelles. *Mol Ther* **15**: 1655–1662.
25. Akagi, D, Oba, M, Koyama, H, Nishiyama, N, Fukushima, S, Miyata, T *et al.* (2007). Biocompatible micellar nanovectors achieve efficient gene transfer to vascular lesions without cytotoxicity and thrombus formation. *Gene Ther* **14**: 1029–1038.
26. Sagara, K and Kim, SW (2002). A new synthesis of galactose-poly(ethylene glycol)-polyethylenimine for gene delivery to hepatocytes. *J Control Release* **79**: 271–281.
27. Brissault, B, Kichler, A, Leborgne, C, Danos, O, Cheradame, H, Gau, J *et al.* (2006). Synthesis, characterization, and gene transfer application of poly(ethylene glycol-b-ethylenimine) with high molar mass polyamine block. *Biomacromolecules* **7**: 2863–2870.
28. Tabata, Y and Ikada, Y (1988). Effect of the size and surface charge of polymer microspheres on their phagocytosis by macrophage. *Biomaterials* **9**: 356–362.
29. Midoux, P, Mayer, R and Monsigny, M (1995). Membrane permeabilization by alpha-helical peptides: a flow cytometry study. *Biochim Biophys Acta* **1239**: 249–256.
30. Uchida, S, Itaka, K, Chen, Q, Osada, K, Miyata, K, Ishii, T *et al.* (2011). Combination of chondroitin sulfate and polyplex micelles from Poly(ethylene glycol)-poly{N'-[N-(2-aminoethyl)-2-aminoethyl]aspartamide} block copolymer for prolonged *in vivo* gene transfection with reduced toxicity. *J Control Release* **155**: 296–302.
31. Vernier, PT, Sun, Y and Gundersen, MA (2006). Nanoelectropulse-driven membrane perturbation and small molecule permeabilization. *BMC Cell Biol* **7**: 37.
32. Beyerle, A, Merkel, O, Stoeger, T and Kissel, T (2010). PEGylation affects cytotoxicity and cell-compatibility of poly(ethylene imine) for lung application: structure-function relationships. *Toxicol Appl Pharmacol* **242**: 146–154.
33. Takae, S, Miyata, K, Oba, M, Ishii, T, Nishiyama, N, Itaka, K *et al.* (2008). PEG-detachable polyplex micelles based on disulfide-linked block catiomers as bioresponsive nonviral gene vectors. *J Am Chem Soc* **130**: 6001–6009.
34. Mitsui, M, Nishikawa, M, Zang, L, Ando, M, Hattori, K, Takahashi, Y *et al.* (2009). Effect of the content of unmethylated CpG dinucleotides in plasmid DNA on the sustainability of transgene expression. *J Gene Med* **11**: 435–443.

Biomaterials 33 (2012) 4722–4730

Contents lists available at SciVerse ScienceDirect

Biomaterials

journal homepage: www.elsevier.com/locate/biomaterials

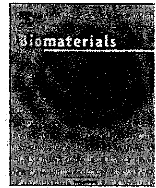

Homo-catiomer integration into PEGylated polyplex micelle from block-catiomer for systemic anti-angiogenic gene therapy for fibrotic pancreatic tumors

Qixian Chen [a], Kensuke Osada [a,**], Takehiko Ishii [b], Makoto Oba [c], Satoshi Uchida [d], Theofilus A. Tockary [a], Taisuke Endo [a], Zhishen Ge [a], Hiroaki Kinoh [a], Mitsunobu R. Kano [e], Keiji Itaka [d], Kazunori Kataoka [a,b,d,*]

[a] Department of Materials Engineering, Graduate School of Engineering, The University of Tokyo, 7-3-1 Hongo, Bunkyo-ku, Tokyo 113-8656, Japan
[b] Department of Bioengineering, Graduate School of Engineering, The University of Tokyo, 7-3-1 Hongo, Bunkyo-ku, Tokyo 113-0033, Japan
[c] Department of Clinical Vascular Regeneration, Graduate School of Medicine, The University of Tokyo, 7-3-1 Hongo, Bunkyo-ku, Tokyo 113-8655, Japan
[d] Division of Clinical Biotechnology, Center for Disease Biology and Integrative Medicine, Graduate School of Medicine, The University of Tokyo, 7-3-1 Hongo, Bunkyo-ku, Tokyo 113-0033, Japan
[e] Department of Molecular Pathology, Graduate School of Medicine, The University of Tokyo, 7-3-1 Hongo, Bunkyo-ku, Tokyo 113-8655, Japan

ARTICLE INFO

Article history:
Received 9 February 2012
Accepted 4 March 2012
Available online 22 March 2012

Keywords:
DNA
Micelle
Nanoparticle
Gene transfer
In vitro test
In vivo test

ABSTRACT

Homo-poly{N′-[N-(2-aminoethyl)-2-aminoehtyl]aspartamide} [PAsp(DET), **H**] was attempted to integrate into poly (ethylene glycol) (PEG)-*b*-PAsp(DET)] (**B**) formulated polyplex micelle with the aim of enhancing cell transfection efficiency for PEGylated polyplex micelle via **H** integration. *In vitro* evaluations verified **H** integration of potent stimulation in enhancing cell-transfecting activity of PEGylated polyplex micelles via promoted cellular uptake and facilitated endosome escape. *In vivo* anti-angiogenic tumor suppression evaluations validated the feasibility of **H** integration in promoting gene transfection to the affected cells via systemic administration, where loaded anti-angiogenic gene remarkably expressed in the tumor site, thereby imparting significant inhibitory effect on the growth of vascular endothelial cells, ultimately leading to potent tumor growth suppression. These results demonstrated potency of **H** integration for enhanced transfection activity and potential usage in systemic applications, which could have important implications on the strategic use of **H** integration in the non-viral gene carrier design.
© 2012 Elsevier Ltd. All rights reserved.

1. Introduction

In recent years, development of non-viral gene delivery carriers has been highlighted with respect to their advantages in low host immunogenicity and large-scale manufacturing [1,2]. Cationic gene carriers, which are formulated through electrostatic self-assembly of anionic plasmid DNA (pDNA) and cationic materials (e.g. polycations, cationic lipids), have emerged as a tempting gene delivery modality in view of their tremendous potential to circumvent ensemble of predefined biological barriers via engineering their chemistry [3]. The principle design criteria in view of the barriers encountered in delivery of exogenous gene to the targeted cells include the abilities of protecting encapsulated pDNA from enzymatic degradation, preventing undesired non-specific interactions in the biological environment, readily being internalized into the affected cells and retrieving from endosome entrapment [4]. To these required principles, we have developed a multibiofunctional catiomer, poly{N′-[N-(2-aminoethyl)-2-aminoehtyl] aspartamide} PAsp (DET) (**H**) [5–8]. This PAsp(DET) catiomer featured as the flanking ethylenediamine moiety in the side chain of N-substituted polyaspartamide (PAsp), displayed distinctive two-step protonation behavior in response to pH gradient, where the protonation of ethylenediamine is facilitated in acidic pH. Interestingly, this acid-responsive trait of PAsp(DET) elicits a selective endosome membrane destabilization function. In contrast to minimal membrane destabilization at physiological pH, fully protonated PAsp(DET) in acidic endosome milieu exerts strikingly explosive destabilization power on cellular membrane, accordingly results in liberation of embedded gene from endosome entrapment to the cytosol and efficient gene transfection without penalty in cell viability [6,9,10]. Still, PAsp(DET) that remains in the cytosol will not provoke cumulative cytotoxic concern due to its appreciable self-catalytic degradable nature, consequently allowing safe gene expression in the affected cells [7].

* Corresponding author. Department of Materials Engineering, Graduate School of Engineering, The University of Tokyo, 7-3-1 Hongo, Bunkyo-ku, Tokyo 113-0033, Japan. Tel.: +81 3 5841 7138; fax: +81 3 5841 7139.
** Corresponding author. Tel.: +81 3 5841 1654; fax: +81 3 5841 7139.
E-mail addresses: osada@bmw.t.u-tokyo.ac.jp (K. Osada), kataoka@bmw.t.u-tokyo.ac.jp (K. Kataoka).

0142-9612/$ – see front matter © 2012 Elsevier Ltd. All rights reserved.
doi:10.1016/j.biomaterials.2012.03.017

On the other hand, it is well acknowledged that direct use of homo-catiomer formulations in systemic therapy was limited since they can readily interact with charged components in the blood stream, in consequence subjected to rapidly clearance by reticuloendothelial system or macrophage cells. To improve the biocompatibility and bioavailability of **H** formulation, surface modification of polyion complex with poly(ethylene glycol) (PEG) was developed via complexation of block-catiomer PEG-*b*-PAsp(DET) (**B**) with pDNA, where single pDNA can be packaged into nanosized core covered by the hydrophilic and biocompatible PEG corona [5]. With merits of this PEG shielding shell, non-specific interactions with biological components were minimized and allows for well dispersing in the blood fluid to stealthily circulate [11]. However, PEG shell reduces affinity to cell membrane so that transfection efficiency extends significance for the ultimate therapeutic potency. In light of dramatic high cell-transfecting activity mediated by homo-PAsp(DET) (**H**) compared to **B** [12], we are encouraged to integrate **H** into **B** based polyplex micelle in pursuit of enhancement for the cell transfection efficiency of PEGylated polyplex micelle in virtue of **H** integration and ultimately achieving improved drug efficacy at the targeted site via systemic administration. Indeed, our recent study has validated feasibility of such block copolymer and homo polymer combined polyplex micelles (**BHPMs**) with pronounced enhancement in transfection efficiency via intratracheal lung administration and remarkably reduced inflammatory response due to inactivated macrophage recognition to polyplexes with PEG shielding [13].

In the present work, we studied the functionalities of **H** integration to PEGylated polyplex micelle and identified the most appreciable combinatorial ratio of **B** and **H** for systemic application. The identified **BHPM** containing anti-angiogenic gene was utilized for treatment of pancreatic tumor bearing mice to demonstrate the utility of **BHPM** for systemic anti-angiogenic tumor therapy.

2. Materials and methods

2.1. Materials

α-Methoxy-ω-amino-poly(ethylene glycol) (M_w 12,000) was obtained from Nippon Oil and Fats Co., Ltd. (Tokyo, Japan). β-Benzyl-L-aspartate N-carboxyanhydride (BLA-NCA) was obtained from Chuo Kaseihin Co., Inc. (Tokyo, Japan). Diethylenetriamine (DET), N,N-dimethylformamide (DMF), n-butylamine, dichloromethane, benzene, and trifluoroacetic acid were purchased from Wako Pure Chemical Industries, Ltd. Alexa-488 succinimidyl ester was a product of Invitrogen (Carlsbad, CA). Fetal bovine serum (FBS) was purchased from Dainippon Sumitomo Parma Co., Ltd. (Osaka, Japan). The pDNAs, pBR322 (4,363 bp) and pGL3 control vector (5,256 bp) were purchased from Takara Bio Inc. (Otsu, Japan). The pDNA encoding luciferase with a CAG promoter provided by RIKEN Gene Bank (Tsukuba, Japan) was amplified in competent DH5α *Escherichia coli* and purified with a QIAGEN HiSpeed Plasmid MaxiKit (Germantown, MD). Cell culture lysis buffer and luciferase Assay System Kit was purchased from Promega Co. (Madison, WI). The Micro BCA™ Protein Assay Reagent Kit was purchased from Pierce Co., Inc. (Rockford, IL). The pDNA encoding a soluble form of VEGF receptor-1 (sFlt-1) was a kind gift from Prof. Masabumi Shibuya in Tokyo Medical and Dental University, and was prepared as previously reported [14]. Dulbecco's modified Eagle's medium (DMEM) was purchased from Sigma–Aldrich (St. Louis, MO). For cellular uptake and intracellular distribution assay, pDNA was labeled with Cy5 using a Label IT Nucleic Acid Labeling Kit from Mirus Bio Corporation (Madison, WI) according to the manufacturer's protocol. Human hepatoma cells (HuH-7) and human umbilical vein endothelial cells (HUVEC) were obtained from the Japanese Collection of Research Bioresources Cell Bank (Tokyo, Japan) and Lonza Ltd. (Basel, Switzerland), respectively. BALB/c nude mice (female, 5 weeks old) were purchased from Charles River Laboratories (Tokyo, Japan). All animal experimental protocols were established according to the guidelines of the Animal Committee of the University of Tokyo.

2.2. Synthesis of B and H

B and **H** were prepared according to a ring-opening polymerization scheme as previously reported [5,7]. In brief, the polymerization of monomer BLA-NCA was initiated from the ω-NH_2 terminal group of α-methoxy-ω-amino-poly (ethylene glycol) (M_w 12,000) (for block-catiomer, **B**) or *n*-butylamine (for homo-catiomer, **H**) to obtain PEG-PBLA or PBLA, respectively, followed by aminolysis reaction to introduce diethylenetriamine molecules into the side chain of PBLA. The prepared polymers were determined to have a narrow unimodal molecular weight distribution (**B**: $M_w/M_n = 1.05$; **H**: $M_w/M_n = 1.06$) by gel permeation chromatography. The polymerization degree of PAsp(DET) segment in **B** was confirmed to be 61 from the peak intensity ratio of the methylene protons in PEG (-OCH_2CH_2-, $\delta = 3.7$ ppm) to the methylene groups in the bis-ethylamine of PAsp(DET): $NH_2(CH_2)_2NH(CH_2)_2NH$- $\delta = 3.1–3.5$ ppm settled in the side chain in the ^1H NMR spectrum in D_2O at 25 °C. The polymerization degree of **H** was confirmed to be 55 according to the peak intensity ratio of the protons of the butyl group at the α-chain end CH_3- to the methylene groups in the bis-ethylamine of PAsp(DET) in the ^1H NMR spectrum in D_2O at 25 °C.

2.3. Preparation of BHPMs

Synthesized **B** and **H** powders were separately dissolved in 10 mM HEPES buffer (pH 7.4) as stock solution. Mixture of **B** and **H** stock solutions at varying **B/H** ratios (residual molar ratio of amino groups in **B** and **H**) was added to pDNA solution for complexation at varying N/P ratios (residual molar ratio of total amino groups in **B** and **H** to phosphate groups in pDNA), followed by overnight incubation at 4 °C. The final concentration of pDNA in all the samples was adjusted to 33.3 μg/mL. Note that all the pre-experimental procedures involved with polymer solution or complex solution were strictly carried out at low temperature, e.g. 4 °C refrigerator or ice bath to avoid polymer degradation [7]. Polyplex micelle formulated from **B** and pDNA was referred hereafter as **B100**, and polyplex formulated from **H** and pDNA was referred hereafter as **H100**.

2.4. Dynamic light scattering

The size and polydispersity index (PDI) of **BHPMs** were determined from the dynamic light scattering (DLS) measurement by the Zetasizer nanoseries (Malvern Instruments Ltd., UK) at a detection angle of 173° and a temperature of 25 °C. **BHPMs** were prepared as described above for three times measurement. The data derived from the rate of decay in the photon correlation function were treated from a cumulant method, and the corresponding diameter of each sample was calculated according to the Stokes–Einstein equation [15].

2.5. Zeta potential

The zeta potential of **BHPMs** was determined from the laser-doppler electrophoresis using the Zetasizer nanoseries (Malvern Instruments Ltd., UK). According to the obtained electrophoretic mobility, the zeta potential of each sample ($n = 3$) was calculated according to the Smoluchowski equation: $\zeta = 4\pi\eta\nu/e$, where η is the viscosity of the solvent, ν is the electrophoretic mobility, and e is the dielectric constant of the solvent.

2.6. Transmission electron microscopy (TEM) measurement

TEM observation was conducted using an H-7000 electron microscope (Hitachi, Tokyo, Japan) operated at 75 kV acceleration voltages for insight on the morphology of **BHPMs** containing pBR322 pDNA. Copper TEM grids with carbon-coated collodion film were glow-discharged for 10 s using an Eiko IB-3 ion coater (Eiko Engineering Co. Ltd., Japan). The grids were dipped into desired **BHPM** solution, which was pre-mixed with uranyl acetate solution (2% (w/v)), for 30 s. The sample grids were blotted by filter paper to remove excess complex solution, followed by air-drying for 30 min. The morphology of the prepared **BHPMs** was determined from the TEM images obtained by staining pDNA with uranyl acetate (UA). Note that PEG shell is invisible under TEM due to its low affinity with UA. Thus, the contours of pDNA strands in the complex were selectively visualized without interference from PEG moieties surrounding pDNA strands. The obtained TEM image was further analyzed by Image J 1.44 (National Institutes of Health) to quantify the length of major axis in each sample, and 100 individual nanoparticles were measured for distribution.

2.7. Binding numbers of B and H to pDNA in BHPMs

The binding behaviors of **B** and **H** to pDNA in each **BHPM** were investigated according to a preparative ultracentrifuge method. As reported previously [14], ultracentrifugation of complex solution allows selective sedimentation of polyplex micelles, while unbound free polymers remain in the supernatant. In consequence, the binding fraction of polymer can be determined by subtracting free polymer (remain in the supernatant after sedimentation) from the total fed polymer. For instance, to quantify the associating number of **B** in the **BHPMs**, Alexa-488 labeled **B** (labeling procedures according to protocol provided by the manufacture, conjugation efficiency: 0.41 Alexa-488 molecules per **B**) and non-labeled **H** were used to prepare a class of **BHPMs** at varying **B/H** ratio, N/P 8 with pDNA (pGL3 control vector). After overnight incubation at 4 °C, 500 μL aliquot of each **BHPM** solution was injected into thickwall polycarbonate tube, 343776 (Beckman Coulter, Inc., Fullerton, CA) and subjected to ultracentrifugation (Optima TLX, Beckman Coulter, Inc., Fullerton, CA) equipped with TLA-120.1 rotor for 3 h under 50,000 g for complete

sedimentation of **BHPMs**. The supernatant with the content of free **B** was collected for fluorescence intensity measurement using a spectrofluorometer (ND-3300, NanoDrop, Wilmington) with an excitation wavelength of 470 nm and an emission wavelength of 519 nm. The concentration of free **B** in the supernatant or the fed **B** solution prior to ultracentrifugation was determined from the obtained fluorescence intensity according to a calibration curve from Alexa488-labeled **B** solutions. Same method was applied to determine the binding number of **H** (conjugation efficiency: 0.34 Alexa-488 molecules per **H**) to pDNA.

2.8. *In vitro transfection efficiency*

HuH-7 cells were seeded on 24-well culture plates (20,000 cells/well) and incubated overnight in 400 μL of DMEM containing 10% FBS in a humidified atmosphere with 5% CO_2 at 37 °C. The medium was replaced with 400 μL of fresh medium, followed by addition of 30 μL each **BHPM** solution (prepared at N/P 8, 1 μg pDNA/well). After 24 h incubation, the medium was exchanged with 400 μL fresh DMEM, followed by another 24 h incubation. The cells were washed with 400 μL of PBS, and lysed in 150 μL of the cell culture lysis buffer. The luciferase activity of the lysates was evaluated from the photoluminescence intensity using Mithras LB 940 (Berthold Technologies, USA). The obtained luciferase activity was normalized according to corresponding amount of proteins in the lysates determined by the Micro BCATM Protein Assay Reagent Kit.

2.9. *Cellular uptake*

Cellular uptake efficiency was evaluated by flow cytometry (BD LSR II, BD, Franklin Lakes, NJ). Cy5-labeled pDNA were used to prepare a group of **BHPMs**. HuH-7 cells were seeded on 6-well culture plate (100,000 cells/well) and incubated overnight in 2 mL of DMEM containing 10% FBS. The medium was replaced with fresh medium, followed by addition of 150 μL **BHPM** solution (33.3 μg pDNA/mL) into each well. After 24 h incubation, the cells were washed 3 times with PBS to remove extracellular Cy5 fluorescence. After detachment by trypsin from the culture plate, the cells were harvested and re-suspended in PBS for flow cytometry measurement.

2.10. *Intracellular distribution*

Endosome escape capacity was determined by evaluating colocalization degree of pDNA and endosome by Confocal laser scanning microscopy (CLSM). In brief, Cy5-labeled pDNA were used to prepare a class of **BHPMs** at N/P 8. HuH-7 cells (50,000 cells) were seeded on 35 mm cell culture dishes and incubated overnight in 1 mL of DMEM containing 10% FBS. The medium was replaced with fresh medium, followed by addition of 75 μL **BHPM** solution (33.3 μg pDNA/mL) into each cell culture dishes. After 24 h incubation, the medium was removed and the cells were rinsed three times with PBS prior to the imaging. The intracellular distribution of each **BHPM** was observed by CLSM after staining acidic late endosomes and lysosomes with LysoTracker Green (Molecular Probes, Eugene, OR) and nuclei with Hoechst 33342 (Dojindo Laboratories, Kumamoto, Japan). The CLSM observation was performed using LSM 510 (Carl Zeiss, Germany) with a 63 × objective (C-Apochromat, Carl Zeiss, Germany) at excitation wavelengths of 488 nm (Ar laser), 633 nm (He-Ne laser), and 710 nm (MaiTai laser for 2-photon imaging) for LysoTrakcer Green (green), Cy5 (red), and Hoechst 33342 (blue), respectively. The colocalization ratio was calculated as previously described [9,12,14] according to the formula:

Colocalization ratio = number of yellow pixels/number of yellow and red pixels,

where yellow corresponds to the pDNA that is trapped into endosome, while red corresponds to the pDNA that is released into the cytosol.

2.11. *Release of **H** in endosome milieu*

A group of **BHPMs** containing pGL3 control vector was prepared with Alexa488-labeled **H** at varying **B**/**H** ratio, N/P 2 (approximate stoichiometric charge ratio) in 10 mM HEPES buffer (pH 7.4). After overnight incubation at 4 °C, aliquot of each **BHPM** solution was mounted by 50 mM acetic acid/acetic sodium buffer (the final pH was adjusted to be 5 for mimicking endosome milieu), followed by another 48 h incubation at 4 °C. The released number of **H** from each **BHPM** was quantified by preceding ultracentrifuge measurement. The releasing percentage was calculated according to the formula:

Released **H** (%) = $(\mathbf{H_{7.4}} - \mathbf{H_5})/\mathbf{H_{7.4}} \times 100$ (%)

where $\mathbf{H_{7.4}}$ denotes associating number of **H** on a pDNA at pH 7.4, and $\mathbf{H_5}$ denotes associating number of **H** on a pDNA after 48 h incubation of **BHPMs** at pH 5.

2.12. *Cell viability*

HuH-7 cells or HUVEC were seeded in 24-well culture plates (20,000 cells/well) and incubated overnight in 400 μL DMEM supplemented with 10% FBS (or MCDB131 containing 10% FBS and 10 ng/mL b-FGF for HUVEC). The medium was replaced with 400 μL of fresh medium, followed by addition of 30 μL each **BHPM** solution into each well (1 μg pDNA/well). After 24 h incubation at 37 °C, the medium was changed to 400 μL of fresh medium, followed by another 24 h incubation. The cells were washed with 400 μL, and cell viability was determined using the Cell Counting Kit-8 (Dojindo, Kumamoto, Japan) according to the manufacturer's protocol. Each well in 200 μL fresh medium was reacted with 20 μL Cell Counting Kit-8 Agent. After 2 h reaction at 37 °C, the absorbance at 450 nm of the formazan in each well was quantified from a microplate reader (Model 680, Bio-rad, UK). The cell viability in each well was calculated and presented as a percentage of control wells without any addition.

2.13. *Tumor suppression efficacy*

BALB/c nude mice were inoculated subcutaneously with BxPC3 cells (5×10^6 cells in 100 μL of PBS). Tumors were allowed to grow for 3 weeks till proliferative phase (the size of the tumors was approximately 50 mm^3). Subsequently, each sample (20 μg sFlt-1 pDNA/mouse) in 10 mM HEPES buffer (pH 7.4) with 150 mM NaCl was intravenously injected via the tail vein 3 times on days 0, 4 and 8. Tumor size was measured every two or three days by a digital vernier caliper across its longest (a) and shortest diameters (b), and its volume (V) was calculated according to the formula $V = 0.5\ ab^2$. Tumor progression was evaluated in terms of relative tumor volume (to day 0) over a period of 28 days, $n = 6$.

2.14. *Vascular density*

BHPMs loading either sFlt-1 or Luc pDNA (20 μg of pDNA) were intravenously injected into the BxPC3-inoculated mice though the tail vein on days 0 and 4. Mice were sacrificed on day 6, and the tumors were excised, frozen in dry-iced acetone, and sectioned into 10 μm thick slices with a cryostat. Vascular endothelial cells (VECs) were immunostained by rat monoclonal antibody antiplatelet endothelial cell adhesion molecule-1 (PECAM-1) (BD Pharmingen, Franklin Lakes, NJ), followed by incubation with Alexa Fluor 488-conjugated secondary antibody. The immunostained sections were observed with CLSM (Carl Zeiss, Germany). The vascular density was quantified by counting the percentage area of PECAM-1-positive pixels per image with 15 images per sample.

2.15. *sFlt-1 expression in the tumor site*

BHPMs loading sFlt-1 (20 μg of pDNA) were intravenously injected into the BxPC3-inoculated mice via the tail vein. Mice were sacrificed at 48 h after injection. The tumors were excised, frozen in dry-iced acetone, and sectioned into 10 μm thick slices with a cryostat. VECs were immunostained using antibodies anti-mouse PECAM-1 (BD Pharmingen, USA) and anti-human and mouse VEGFR1 (ab32152, Abcam Japan, Tokyo, Japan). The sections immunostained was observed with CLSM (Carl Zeiss, Germany). The sFlt-1 gene expression was quantified by counting the percentage area of ab32152-positive pixels per image with 6 images per sample.

3. Results and discussion

3.1. *Characterizations of **BHPMs***

One of most important factors for developing gene delivery carriers is possession of nanosized dimensions and stealth surface characteristics to enable circulation in the blood stream to the targeted tissue. In this respect, the size and zeta potential of **BHPMs** were examined. From the size characterization by DLS, all **B**-included samples presented cumulant diameters ranging from 60 nm to 100 nm (Supplementary Table S1) with unimodal size distributions of low PDI from 0.1 to 0.2 (Supplementary Table S2), whereas **H100** presented remarkably larger size over 1000 nm at a critical N/P range of 1.5–2. In the range over this critical N/P range (N/P ≥ 2), **H100** possessed comparable size of approximate 75 nm with unimodal size distribution.

The zeta potential of **BHPMs** was examined because possession of neutral zeta potential is necessary to diminish non-specific interactions with biological components, protein adsorption, aggression, opsonization [16,17]. For this purpose, the zeta potential of **BHPMs** was examined. Overall, negative net charge of pDNA in all complexes was approximately neutralized at a critical N/P of 1.5–2, which is consistent with the protonation degree (53%) of amino groups in PAsp(DET) at neutral pH 7.4 [5]. This suggests aforementioned large-sized formulation of **H100** at this critical N/P range may form through the secondary aggregation of the charge neutralized polyplexes. In the range above this critical N/P range, **H100** (N/P ≥ 2) possessed remarkable positive value in zeta potential approximate +40 mV (Supplementary Table 3). On the

contrary, the zeta potential of **B100** was significantly suppressed to neutral approximate +5–6 mV, indicating charge-masking effect of PEGylation from **B**. To our interests, the neutral zeta potential remained for the **BHPMs** with **H**% ≤ 50%, though **BHPM** at **B/H** = 75/25 showed higher zeta potential (over +10 mV) possibly ascribe to insufficient PEG shielding due to low **B** content. Each group of **BHPMs** with same **H**% (over than stoichiometric charge ratio, N/P ≥ 2) showed comparable size and zeta potential regardless of N/P ratios. Here, we choose **BHPMs** prepared at N/P 8 as representative for hereafter investigations.

The morphology of **BHPMs** was investigated by TEM measurement (Fig. 1). Note that pDNA strands in the **BHPMs** were selectively observed in the TEM image due to stronger affinity of uranyl acetate (UA) to DNA compared to PEG. **B100** presents as uniform rod-shaped particles (Fig. 1a), suggesting DNA strand is packaged into the rod-shaped bundle through a regular folding behavior [18]. In contrast, **H100** in absence of PEG surface tethering adopted a completely collapsed spherical configuration (Fig. 1d). This stark contrast implied the crucial role of the tethered PEG chains in mediating pDNA packaging. To obtain this collapsed spherical configuration using **B**, the tethered PEG chains must be stuffed as a corona surrounding the spherical core. Apparently, this PEG crowding hinders segmental motion of PEG chains, which is unfavorable with respect to conformational entropy. Hence, it is reasonable to assume that osmotic pressure caused by the crowded PEG chains sustains pDNA collapsing induced by PAsp(DET) binding. Presumably, the tethered PEG may regulate pDNA packaging configurations. According to this discipline, an intermediate pDNA packaging configuration may reside in **BHPMs** by reducing tethered PEG chains. The TEM observations approved our speculations and revealed progressive pDNA configuration change from rod to ellipsoid with shortened length of major axis (58 nm - 44 nm, Fig. 1e) in **BHPMs** along a decreasing content of **B** (Fig. 1b and c) and ultimately collapsed into spherical configuration in the absence of **B** (**H100**). This tendency coincides with the prior DLS measurement, where smaller size and lower PDI were obtained at lower **B**%. Of note, this **B/H** ratio dependent manner in pDNA packaging configuration implies the binding content of **B** and **H** to pDNA relies on the fed **B/H** ratios.

To gain direct insight on the binding fashions of **B** and **H** to pDNA, the compositions of **B** and **H** in **BHPMs** were quantified according to ultracentrifuge technique. In principle, appropriate ultracentrifugal field was applied for selective sedimentation of complexes, whereas unbound polymer to pDNA (free polymer) stays in the solution. Appending fluorescence dye to **B** (vice versa for **H**), the binding compositions of **B** can be quantified by comparing the total fed number of **B** and the free number of **B**. Overall, the binding compositions of **B** and **H** in the **BHPMs** remain fairly consistent with the fed **B/H** ratios (Fig. 2a). Interestingly, identical number of amino groups was found for complexation with one pDNA. Since the bound PAsp(DET)s onto a pDNA possessed 20,000 amino groups in total, in which 53% of amino groups (10,600) presumes to be positively charged at pH 7.4, which coincide with the number of phosphate groups in one pDNA (pGL3: 10,652 negative charges from 5,326 bps). All the **BHPMs** appeared to be formulated exclusively according to stoichiometric charge ratio independent on the fed **B/H** ratio. This result provides essential insight on **BHPMs** formulation with the binding ratio of **B** and **H** according to the fed **B/H** ratio, thereby allowing precise control of compositions in **BHPMs** by simply altering the fed **B/H** ratios.

In summary, we have successfully integrated **H** into polyplex micelle and fabricated distinct PEGylated **BHPM** micelle formulation with neutral zeta potential in the range of **H** ≤ 50%. In addition, the composition of **B** and **H** in **BHPM**s can be facile controlled by varying fed **B** and **H** ratio. The biological impacts of **H** integration on PEGylated polyplex micelle were then investigated.

3.2. Enhanced cellular transfection of **BHPMs** from **H** integration

The transfection efficiency of **BHPMs** was evaluated to verify the effect of **H** integration. Notably, **H** integration appeared to significantly enhance transfection efficiency of polyplex micelle, whereas no observable transfection activities were found in **B100** (Fig. 3). In particular, a pronounced jump of transfection efficiency was observed from the point of **H**% of 30%, e.g. **BHPM** at **B/H** = 50/50 capable of mediating comparable high level of transfection efficiency as **H100**. This result approved the powerful potency of **H** integration in enhancing transfection activity of PEGylated polyplex micelle. To understand how **H** integration to PEGylated polyplex micelle worked in transfection, we examined cellular uptake efficiency and endosome escape capacity of **BHPMs** as varying **H**

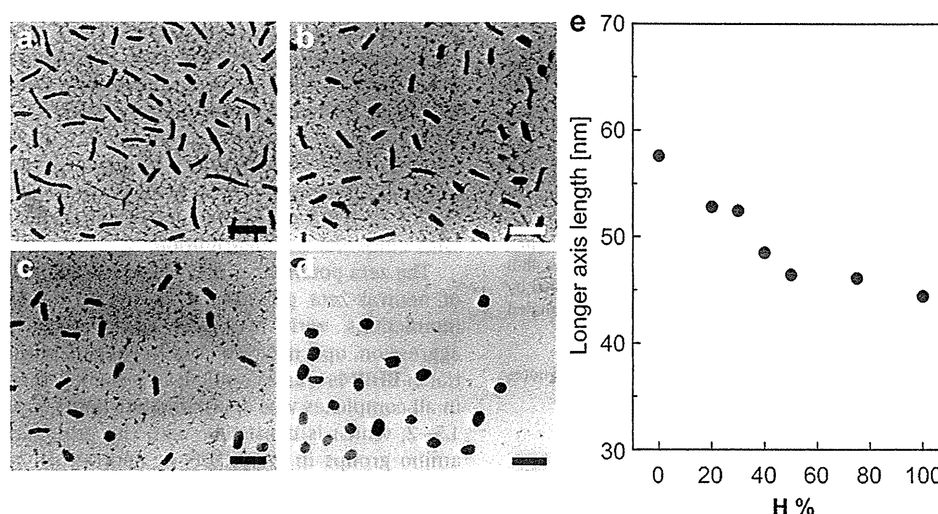

Fig. 1. Morphology of **BHPMs** at varying **H** integration ratio according to TEM observation. a)–d): Representative TEM images of **BHPMs** at varying **H** integration ratio, a) **B/H** = 100/0; b) **B/H** = 70/30; c) **B/H** = 50/50; and d) **B/H** = 0/100. The scale bars represent 100 nm in all TEM images. e) Number average length of major axis of **BHPMs** at varying **H** integration ratio analyzed according to acquired TEM images (n = 100).

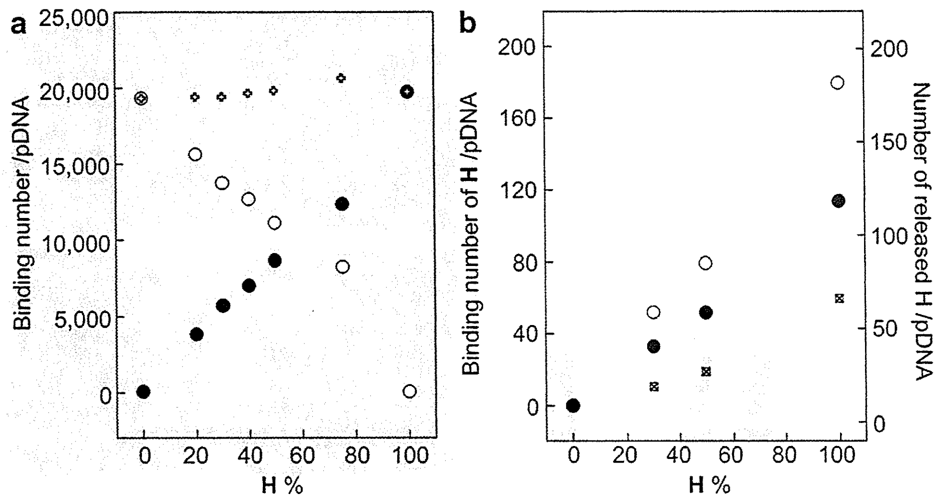

Fig. 2. Binding fashions of **B** and **H** to pDNA in **BHPMs** at varying **H** integration ratio. a): Binding compositions of **B** and **H** in **BHPMs** at pH 7.4. Open circles: **B**; Closed circles: **H**; Open crosses: **B** + **H**. Binding quantity of **B** or **H** in **BHPMs** was expressed as the number of amino groups from associated **B** or **H** per pGL3 pDNA. b): Binding number of **H** chains per pGL3 pDNA at pH 7.4 or pH 5. Open circles: pH = 7.4; Closed circles: pH = 5. Crossed squares: released number of **H** was calculated from comparison of binding numbers of **H** at pH 7.4 and pH 5.

integration ratio because these two events are the crucial factors determining the magnitude of transfection efficiency. The cellular uptake efficiency of **BHPMs** was evaluated by quantifying the internalized pDNA using flow cytometry analysis (Fig. 4a). In consistent with the transfection tendency, no observable cellular uptake was found in **B100**, whereas **BHPMs** exhibited striking contrast with remarkable enhancement in cellular uptake efficiency, e.g. **BHPMs** at **B/H** = 70/30 and 50/50 experienced potent promotion in cellular uptake activity (comparable to **H100**). The

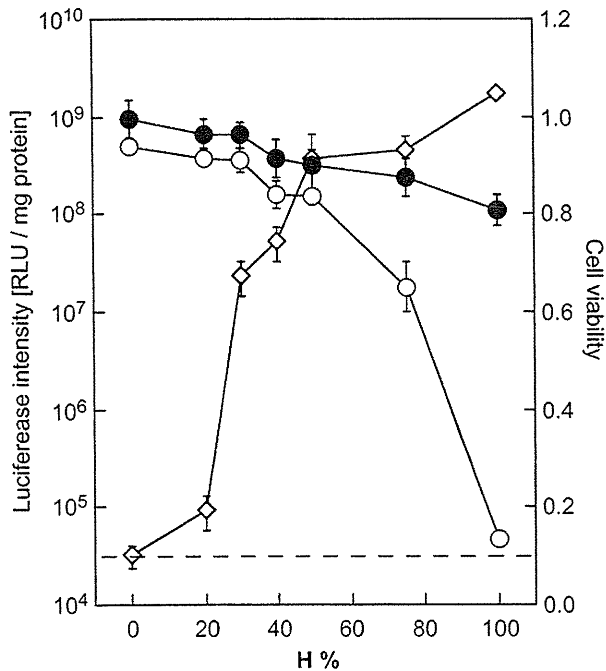

Fig. 3. Transfection efficiency and cell viability of **BHPMs** at varying **H** integration ratio. Dotted line: background level of transfection efficiency in HuH-7. Open diamonds: transfection efficiency of **BHPMs** in HuH-7 cells; Closed circles: cell viability of HuH-7 cells; Open circles: cell viability of HUVEC cells (mean ± SEM, $n = 4$).

results suggest powerful potency of **H** integration in promoting cellular uptake of PEGylated polyplex micelle. Possibly, decrease of PEG chains in the **BHPMs** with increasing **H** content may facilitate cellular uptake because PEGylation reduces affinity of PEGylated nanocarriers to cell adhesion [19,20]. The detailed underlying mechanism for this enhancement in cellular uptake is ongoing.

The internalized **BHPMs** after endocytosis are subjected to endosome entrapment and eventually end up with enzymatic degradation if they cannot afford adequate facilities to retrieve the entrapped gene from late endosome [21]. Hence, intracellular distributions of **BHPMs** were characterized by CLSM observations (Fig. 4). No significant amount of pDNA (stained as red) localized inside the cells for **B100** (Fig. 4b), which is in agreement with flow cytometry result. On the contrary, **BHPMs** at **B/H** = 70/30 and 50/50 and **H100** (Fig. 4c–e) reveals larger amount of pDNA were internalized into the cells than **B100**. Endosome escape capacities of **BHPMs** were studied in term of quantifying colocalization degrees of pDNA and late-endosome/lysosome (green), thus lower colocalization degree represented higher endosome escape capacity. Interestingly, colocalization ratios of **BHPMs** appeared to follow a clear **H** content dependent manner (Fig. 4a), where lower colocalization ratio attained in the **BHPMs** with larger **H** content. This tendency suggests **H** integration played a prominent role in mediating the release of **BHPMs** from endosome entrapment. A plausible reason for this tendency may lean on the potent membrane disrupting activity of **H** in endosome milieu [6]. As we demonstrated previously, the membrane destabilizing capacity of **H** was low at pH 7.4, while it was remarkably high in acidic condition (endosome milieu), which gave rise to substantially enhanced potency of **H** in endosome escape. In light of the fact that **BHPMs** were self-assembled according to stoichiometric charge ratio, it is reasonable to anticipate that some fraction of integrated **H** might be released from **BHPMs** in endosome milieu, which accounts for endosome membrane disruption. At physiological milieu (pH = 7.4), the ethylenediamine side chain of PAsp(DET) takes almost monoprotonated form with the protonation degree of 0.53, while the protonation was facilitated by acidification, e.g. the majority of ethylenediamine side chain takes double protonated form in endosome milieu with the protonation degree of 0.90 (pH = 5) [6]. The promoted protonation of PAsp(DET) would

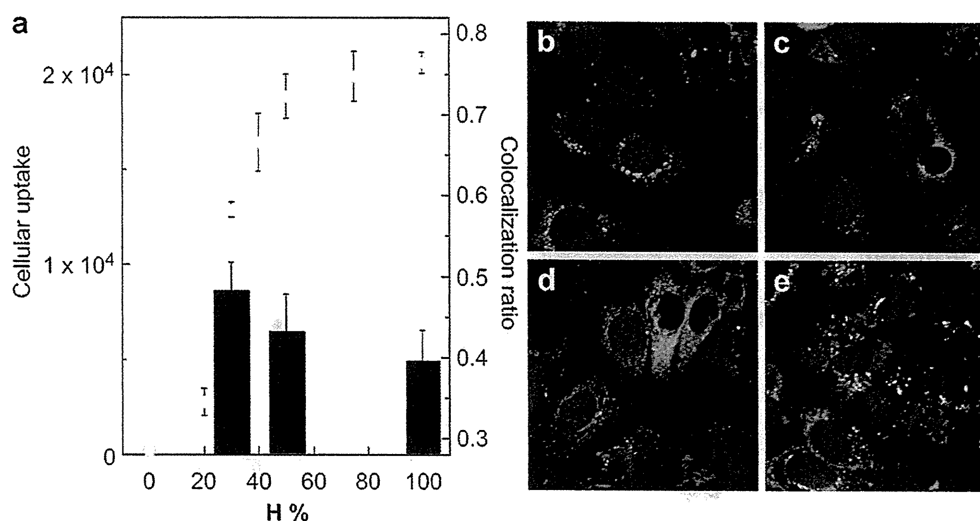

Fig. 4. Cellular uptake and endosome escape profiles of **BHPMs** at varying **H** integration ratio. Open circles: Cellular uptake efficiency of **BHPMs** to HuH-7 cells (mean ± SEM, $n = 3$). b) - e): CLSM images for insight on intracellular distributions of **BHPMs** at varying **H** integration ratio. b) **B/H** = 100/0; c) **B/H** = 70/30; d) **B/H** = 50/50; and e) **B/H** = 0/100. Blue: nucleus; Green: late endosome or lysosome; Red: pDNA. Endosome escape was determined by quantifying colocalization ratio of pDNA and late-endosome/lysosome as summarized in (a) as bar graph (mean ± SEM, $n = 10$). The scale bars represent 10 μm in all CLSM images. (For interpretation of the references to color in this figure legend, the reader is referred to the web version of this article.)

concomitantly elicit transient over-stoichiometric charge for the polyion complex core. Apparently, this transient over-stoichiometric complex are not stable due to the electrostatic repulsion of excessive charged catiomers in the complex and would readily release charged chains in the polyion complex to recover electrostatic equilibrium. For evidence of this speculation, a class of **BHPMs** prepared in the HEPES buffer (pH 7.4) was subjected for pH 5 for mimicking endosome entrapment. The remaining binding numbers of **H** per pDNA in **BHPM** were quantified by ultracentrifuge analysis as aforementioned and compared to original binding numbers of **H** per pDNA at pH 7.4. Fig. 2b approves considerable amount of integrated **H** released from each **BHPM** at pH 5 as compared to that at pH 7.4. The releasing numbers of **H** displayed a clear **H** integration ratio dependent manner, where those **BHPMs** with higher **H%** tend to release more. Accordingly, we may speculate that the releasing fraction of **H** would exert disruption of endosome membrane so that allowing for facilitated endosome escape. Indeed, our recent study has verified **H** of powerful membrane destabilization potency in acidic endosome milieu [13], thus approved **H** integration as a convincing strategy in facilitating pDNA release from endosome entrapment.

Minimizing the cytotoxicity, aside from increasing efficacy, is one of key factors in establishing safer gene carriers which are clinically applicable. In this respect, we assessed cell viability in presence of **BHPMs** for two cell lines. First, cell viability was accessed in HuH-7 cells, which was used in the transfection efficiency evaluations. As shown in Fig. 3, no significant cytotoxicity was observed, suggesting safety of our **BHPMs**. Cytotoxicity was further assessed in HUVEC cell-line, which is more sensitive in terms of toxicity [6], and confirmed minimal cytotoxicity was observed with the **BHPMs** at low **H%** (**H%** ≤ 50%). In particular, cytotoxicity was negligible with **H%** ≤ 30%.

In summary, **H** integration conferred multi-merits in elevating transfection efficiency of PEGylated polyplex micelle, including promoted cellular uptake and facilitated endosome escape. Ultimately, **BHPMs** at **B/H** = 70/30 was identified as the most appreciable **BHPM** comprising high transfection efficiency, minimal cytotoxic profile and charge-shielded surface characters for subsequent systemic gene therapy test.

3.3. Potent tumor growth suppression by treatment with BHPMs

Pancreatic cancer remains one of the highest fatalities among various cancers [22–26] and anti-angiogenic approach is recently

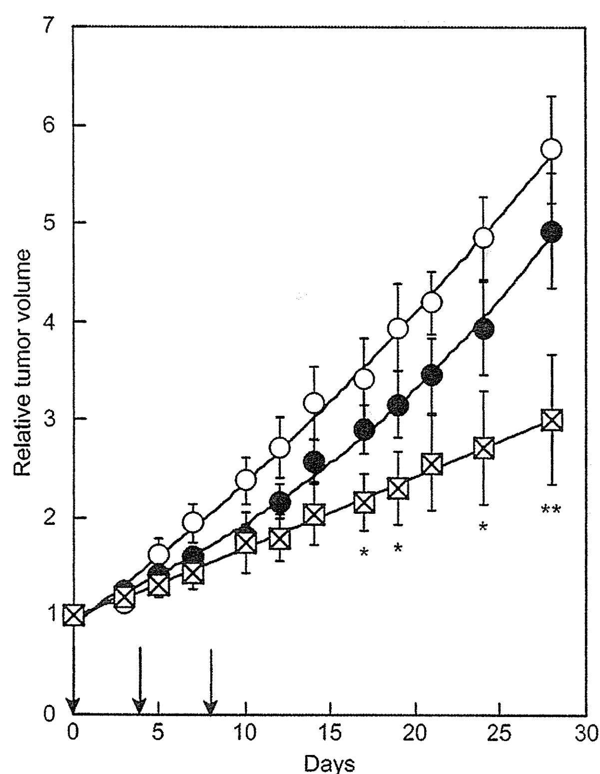

Fig. 5. Antitumor activity of **BHPM** loading sFlt-1 pDNA in subcutaneously BxPC3-inoculated mice via intravenous administration. Open circles: HEPES buffer as control; Closed circles: **B100**; Crossed squares: **BHPM** at **B/H** = 70/30 (mean ± SEM, $n = 6$). Data points marked with asterisks are statistically significance of **BHPM** group relative to both control group and **B100** group (*$P < 0.05$, **$P < 0.01$; Student's t test).

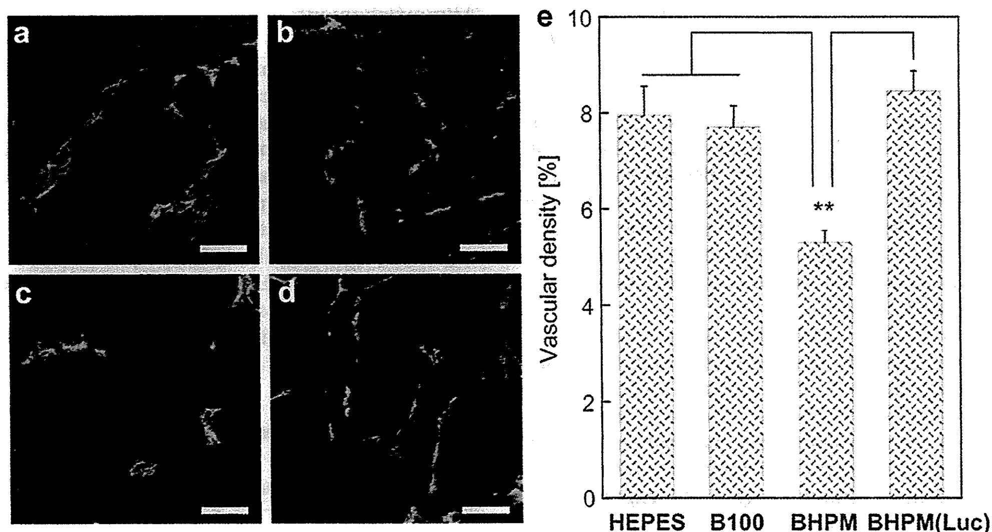

Fig. 6. CLSM image of immunostaining of PECAM-1-positive-vascular endothelial cells in the BxPC3 tumor tissue. a) HEPES; b) **B100** loading sFlt-1 pDNA; c) **BHPM** (**B**/**H** = 70/30) loading sFlt-1 pDNA; and d) **BHPM** (**B**/**H** = 70/30) loading Luc pDNA. The scale bars represent 100 μm in all CLSM images. e) Areas of PECAM-1-positive region (green) quantified from CLSM images (mean ± SEM, $n = 15$; $^{**}P < 0.01$, Student's *t* test). (For interpretation of the references to color in this figure legend, the reader is referred to the web version of this article.)

thought to be a promising way to treat this type of cancer [27,28]. Vascular endothelial growth factor (VEGF), a major signaling molecule to stimulate angiogenesis via promoting endothelial cell proliferation and migration [29,30], is one of most intensively used targets for antiangiogenesis tumor therapy [31–33]. Here, we selected pDNA encoding soluble VEGF receptor-1, or soluble fms-like tyrosine kinase-1 (sVEGFR1, or sFlt-1) [31], which inhibits VEGF signaling by strong binding to VEGF molecules without transducing signals into cells, as payload to test the feasibility of **BHPMs** in systemic applications *in vivo*.

BHPMs at **B**/**H** = 70/30 (simply referred as **BHPMs** hereafter) containing sFlt-1 were intravenously injected into mice bearing pancreatic adenocarcinoma BxPC3 via the tail vein on day 0, 4 and 8. **BHPMs** exerted significantly tumor suppression compared to the

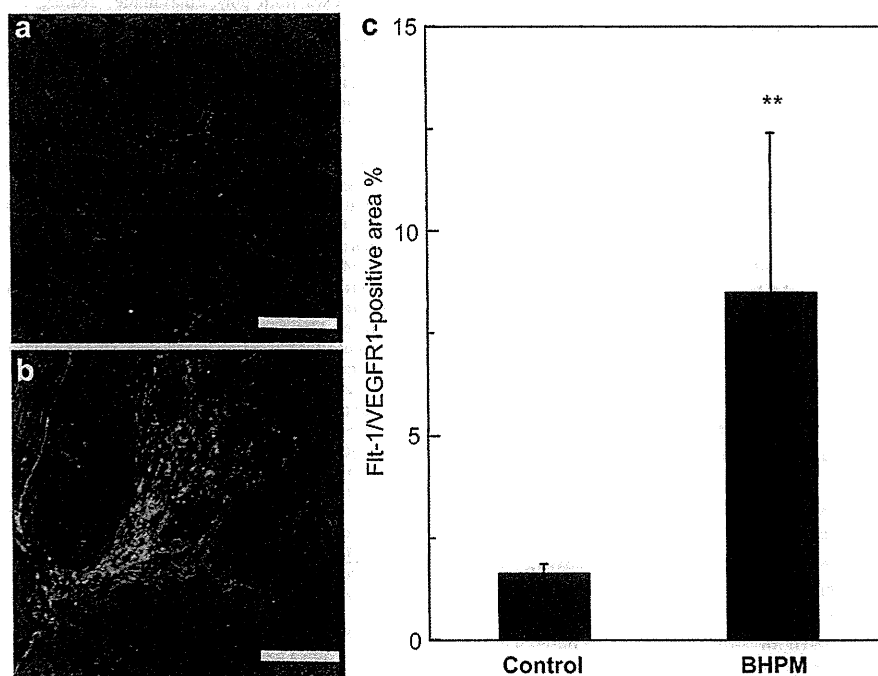

Fig. 7. Expression of sFlt-1 protein by pDNA loaded in **BHPM** (**B**/**H** = 70/30) in the BxPC3 tumor tissue *in vivo*. a) HEPES buffer used as a control. b) **BHPM** (**B**/**H** = 70/30) loading sFlt-1 pDNA. Blue: nucleus; Red: vascular endothelial cells. Green: expressed sFlt-1 (or inherent Flt-1/VEGFR1). The scale bars represent 200 μm in all CLSM images. c) Areas of Flt-1/VEGFR1-positive region (green) were quantified from the images (mean ± SEM, $n = 6$; $^{**}P < 0.01$, Student's *t* test). (For interpretation of the references to color in this figure legend, the reader is referred to the web version of this article.)

mice treated with HEPES buffer (control) and **B100** (*$P < 0.01$, Fig. 5). Moreover, no noticeable side effect appeared in both **B100** and **BHPMs** treated mice, according to mice weight measurement (data not shown). To confirm the inhibited tumor growth due to anti-angiogenic effect, vascular endothelial cells (VECs) was immunostained by using PECAM-1, and quantified. As shown in Fig. 6, vascular density of tumors treated by **BHPMs** was significantly lower than that of the other groups (*$P < 0.01$). Note that the vascular density treated by **BHPMs** loading Luc pDNA was the same as the control group. The result suggests the expression of loaded sFlt-1 pDNA in **BHPMs** suppressed vascular growth, thus led to inhibitory growth of tumor tissue.

To confirm obtained anti-angiogenic effect due to loaded sFlt-1 pDNA expression at the tumor site, we immunostained the tumor tissue using an antibody for Flt-1. The antibody detected both soluble and membrane-bound VEGFR1/Flt-1 for both human and mouse, therefore both overexpressed and naturally expressed VEGFR1/Flt-1 in both mouse tissues and human-derived cancer cells were observable. Still, as shown in Fig. 7, the expression of total VEGFR1/Flt-1 (green) was remarkably higher in the mice administered **BHPMs** compared to control sample. This observation suggested that administration of **BHPMs** enabled effective expression of sFlt-1 in the tumor tissue, in agreement with the observations for vascular density decrease (Fig. 6) and tumor growth suppression (Fig. 5). Moreover, it was found that the expressed sFlt-1 enriched in the tumor stroma adjacent to the vascular endothelial cells (red), rather than the tumor mass (cell nucleus stained into blue). Since BxPC3 pancreatic adenocarcinoma has thick fibrosis [34], possibly sFlt-1 pDNA encapsulated in **BHPMs** may have not directly transfected to the cancer cells in the tumor nests, alternatively, it transfected to the stromal cells adjacent to the vascular lumens (e.g. VECs, fibroblasts). The sFlt-1 proteins secreted from these cells might conduce to potent anti-angiogenic environment for the entrapment of VEGF protein in the tumor site, consequently decreased the growth of vascular endothelial cells and retarded the growth of pancreatic tumor. It should be noted that, as opposed to anti-cancer drug, antiangiogenesis gene therapy delineates a particularly fascinating tool due to no necessity of selective and massive transfer of anti-angiogenic genes into all the cancer cells. Namely, transferring anti-angiogenic genes into the cells merely in the vicinity of the tumor site was able to cause spontaneously local accumulation of anti-angiogenic product in the tumor tissue, although not in tumor nests *per se*, resulted in providing adequate anti-angiogenic environment for tumor regression. Since delivering pharmaceutical agent to all the targeted tumor cells is an onerous task, anti-angiogenic tumor therapy is of particular interests and should be an emphasized strategy in treatment for solid tumor.

4. Conclusions

We have demonstrated the utility of **H** integration into **B** based polyplex micelle that potentiates cellular endocytosis and endosome escape for PEGylated polyplex. Furthermore, the most appreciable **BHPM** according to the perspectives of both safety and efficacy was identified toward systemic anti-angiogenic therapy and has validated the feasibility of **H** integration in creating safe and efficient non-viral systemic gene delivery carrier. **BHPM** loaded by sFlt-1 pDNA imparted potent suppression on tumor growth due to inhibitory growth of tumor vascular endothelial cells by the expression of loaded sFlt-1 gene at the tumor site. Therefore, the use of **BHPMs** by strategically integration of **H** is of great interest to promote gene transfection efficiency and worthy to further develop to find broad utility in gene therapy via systemic route.

Acknowledgments

This work was financially supported by the Core Research Program for Evolutional Science and Technology (CREST) from the Japan Science and Technology Corporation (JST), by the Japan Society for the Promotion of Science (JSPS) through its "Funding Program for World-Leading Innovative R&D on Science and Technology (FIRST Program) and by the Center for Medical System Innovation (CMSI) (Global COE Program, MEXT). Q. C. acknowledges the fellowship from Ministry of Education, Science, Sports and Culture, Japan (MEXT). The authors are grateful to Dr. X. Liu for her technical support and assistance in animal experiment and to Ms. Y. Li and Mr. A. Dirisala for their intellectual contributions to the discussion.

Appendix A. Supplementary data

Supplementary data related to this article can be found online at doi:10.1016/j.biomaterials.2012.03.017.

References

[1] Mastrobattista E, van der Aa MAEM, Hennink WE, Crommelin DJA. Artificial viruses: a nanotechnological approach to gene delivery. Nat Rev Drug Discov 2006;5:115–21.
[2] Mintzer M, Simanek EE. Nonviral vectors for gene delivery. Chem Rev 2009; 109:259–302.
[3] Morille M, Passirani C, Vonarbourg A, Clavreul A, Benoit JP. Progress in developing cationic vectors for non-viral systemic gene therapy against cancer. Biomaterials 2008;29:3477–96.
[4] Osada K, Christie RJ, Kataoka K. Polymeric micelles from poly(ethylene glycol)-poly(amino acid) block copolymer for drug and gene delivery. J R Soc Interface 2009;6:S325–39.
[5] Kanayama N, Fukushima S, Nishiyama N, Itaka K, Jang WD, Miyata K, et al. A PEG-based biocompatible block catiomer with high buffering capacity for the construction of polyplex micelles showing efficient gene transfer toward primary cells. Chem Med Chem 2006;1:439–44.
[6] Miyata K, Oba M, Nakanishi M, Fukushima S, Yamasaki Y, Koyama H, et al. Polyplexes from poly(aspartamide) bearing 1,2-diaminoethane side chains induce pH-selective, endosomal membrane destabilization with amplified transfection and negligible cytotoxicity. J Am Chem Soc 2008;130:16287–94.
[7] Itaka K, Ishii T, Hasegawa Y, Kataoka K. Biodegradable polyamino acid-based polycations as safe and effective gene carrier minimizing cumulative toxicity. Biomaterials 2010;31(13):3707–14.
[8] Kim HJ, Ishii A, Miyata K, Lee Y, Wu S, Oba M, et al. Introduction of stearoyl moieties into a biocompatible cationic polyaspartamide derivative, PAsp(DET), with endosomal escaping function for enhanced siRNA-mediated gene knockdown. J Control Release 2010;145:141–8.
[9] Uchida H, Miyata K, Oba M, Ishii T, Suma T, Itaka K, et al. Odd-even effect of repeating aminoethylene units in the side chain of N-substituted polyaspartamides on gene transfection profiles. J Am Chem Soc 2011;133: 15524–32.
[10] Miyata K, Nishiyama N, Kataoka K. Rational design of smart supramolecular assemblies for gene delivery: chemical challenges in the creation of artificial viruses. Chem Soc Rev 2012;41:2562–74.
[11] Nomoto T, Matsumoto Y, Miyata K, Oba M, Fukushima S, Nishiyama N, et al. In situ quantitative monitoring of polyplexes and polyplex micelles in the blood circulation using intravital real-time confocal laser scanning microscopy. J Control Release 2011;151:104–9.
[12] Takae S, Miyata K, Oba M, Ishii T, Nishiyama N, Itaka K, et al. PEG-detachable polyplex micelles based on disulfide-linked block catiomers as bioresponsive nonviral gene vectors. J Am Chem Soc 2008;130:6001–9.
[13] Uchida S, Itaka K, Chen Q, Osada K, Ishii T, Shibata MA, et al. PEGylated polyplex with optimized PEG shielding enhances gene introduction in lungs by minimizing inflammatory responses. Mol Ther; 2012. doi:10.1038/mt.2012.20.
[14] Oba M, Miyata K, Osada K, Christie RJ, Sanjoh M, Li WD, et al. Polyplex micelles prepared from ω-cholesteryl PEG-polycation block copolymers for systemic gene delivery. Biomaterials 2011;32:652–63.
[15] Harada A, Kataoka K. Formation of polyion complex micelles in an aqueous milieu from a pair of oppositely-charged block copolymers with poly(ethylene glycol) segments. Macromolecules 1995;28:5294–9.
[16] Jones MC, Leroux JC. Polymeric micelles - a new generation of colloidal drug carriers. Eur J Pharm Biopharm 1999;48:101–11.
[17] Otsuka H, Nagasaki Y, Kataoka K. Self-assembly of poly(ethylene glycol)-based block copolymers for biomedical applications. Curr Opin Colloid Interface Sci 2001;6:3–10.

[18] Osada K, Oshima H, Kobayashi D, Doi M, Enoki M, Yamasaki Y, et al. Quantized folding of plasmid DNA condensed with block catiomer into characteristic rod structures promoting transgene efficacy. J Am Chem Soc 2010;132:12343–8.
[19] Mishra S, Webster P, Davis ME. PEGylation significantly affects cellular uptake and intracellular trafficking of non-viral gene delivery particles. Eur J Cell Biol 2004;83:97–111.
[20] Kursa M, Walker GF, Roessler V, Ogris M, Roedl W, Kircheis R, et al. Novel shielded transferrin-polyethylene glycol-polyethylenimine/DNA complexes for systemic tumor-targeted gene transfer. Bioconjug Chem 2003;14:222–31.
[21] Varkouhi AK, Scholte M, Storm G, Haisma HJ. Endosomal escape pathways for delivery of biologicals. J Control Release 2011;151:220–8.
[22] Mancuso A, Calabrò F, Sternberg CN. Current therapies and advances in the treatment of pancreatic cancer. Crit Rev Oncol Hematol 2006;58:231–41.
[23] Freelove R, Walling AD. Pancreatic cancer: diagnosis and management. Am Fam Physician 2006;73:485–92.
[24] Huguet F, Girard N, Guerche CS. Chemoradiotherapy in the management of locally advanced pancreatic carcinoma: a qualitative systematic review. J Clin Oncol 2009;27:2269–77.
[25] Klautke G, Brunner TB. Radiotherapy in pancreatic cancer. Strahlenther Onkol 2008;184:557–64.
[26] Zuckerman DS, Ryan DP. Adjuvant therapy for pancreatic cancer: a review. Cancer 2008;112:243–9.
[27] Folkman J, Bach M, Rowe JW, Davidoff F, Lambert P, Hirsch C, et al. Tumor angiogenesis-therapeutic implications. N Engl J Med 1971;285:1182–6.
[28] Quesada AR, Munoz-Chapuli R, Medina MA. Anti-angiogenic drugs: from bench to clinical trials. Med Res Rev 2006;26:483–530.
[29] Pralhad T, Madhusudan S, Rajendrakumar K. Concept mechanisms and therapeutics of angiogenesis in cancer and other diseases. J Pharm Pharmaco 2003;55:1045–53.
[30] Carmeliet P, Jain RK. Angiogenesis in cancer and other diseases. Nature 2000;407:249–57.
[31] Kong HL, Hecht D, Song W, Kovesdi I, Hackett NR, Yayon A, et al. Regional suppression of tumor growth by in vivo transfer of a cDNA encoding a secreted form of the extracellular domain of the Flt-1 vascular endothelial growth factor receptor. Hum Gene Ther 1998;9:823–33.
[32] Oba M, Vachutinsky Y, Miyata K, Kano MR, Ikeda S, Nishiyama N, et al. Antiangiogenic gene therapy of solid tumor by systemic injection of polyplex micelles loading plasmid DNA encoding soluble Flt-1. Mol Pharm 2010;7:501–9.
[33] Vachutinsky Y, Oba M, Miyata K, Hiki S, Kano MR, Nishiyama N, et al. Antiangiogenic gene therapy of experimental pancreatic tumor by sFlt-1 plasmid DNA carried by RGD-modified crosslinked polyplex micelles. J Control Release 2011;149:51–7.
[34] Cabral H, Matsumoto Y, Mizuno K, Chen Q, Murakami M, Kimura M, et al. Accumulation of sub-100 nm polymeric micelles in poorly permeable tumours depends on size. Nat Nanotech 2011;12:815–23.

Biomaterials 33 (2012) 325–332

Contents lists available at SciVerse ScienceDirect

Biomaterials

journal homepage: www.elsevier.com/locate/biomaterials

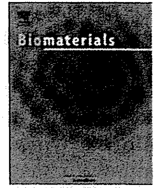

Enhanced gene expression promoted by the quantized folding of pDNA within polyplex micelles

Kensuke Osada[a,c], Tomonori Shiotani[a], Theofilus A. Tockary[a], Daigo Kobayashi[a], Hiroki Oshima[a], Sorato Ikeda[a], Ronald J. Christie[b,c], Keiji Itaka[b,c], Kazunori Kataoka[a,b,c,*]

[a] *Department of Materials Engineering, Graduate School of Engineering, The University of Tokyo, 7-3-1 Hongo, Bunkyo-ku, Tokyo 113-8656, Japan*
[b] *Division of Clinical Biotechnology, Center for Disease Biology and Integrative Medicine, Graduate School of Medicine, The University of Tokyo, 7-3-1 Hongo, Bunkyo-ku, Tokyo 113-8656, Japan*
[c] *Center for NanoBio Integration, The University of Tokyo, 7-3-1 Hongo, Bunkyo-ku, Tokyo 113-8656, Japan*

ARTICLE INFO

Article history:
Received 1 September 2011
Accepted 21 September 2011
Available online 10 October 2011

Keywords:
DNA
Micelle
Nanoparticle
Gene transfer
In vivo test
In vitro test

ABSTRACT

Selective packaging of plasmid DNA (pDNA) into folded rod or collapsed sphere structures in polyplex micelles was demonstrated by modulating the PLys segment length of poly(ethylene glycol)-*block*-poly(L-lysine) (PEG-PLys) block catiomers used for micelle formation. The two basic packaging structures correlated well to the integrity of double-stranded DNA contained within the micelles. Rod structures formed by the quantized folding mechanism, which results in dissociation of double-stranded DNA only at each fold. Collapsed sphere structures formed by substantial random disruption of the double-stranded DNA structure. Analysis of gene expression in a cell-free transcription/translation system, cultured cells and also skeletal muscle of mice showed that micelles containing pDNA packaged by quantized folding exhibited higher gene expression than naked pDNA and micelles containing collapsed pDNA. These results indicate that controlled packaging of pDNA into an appropriate structure is critical for achieving effective gene expression. Improved gene transfection and expression resulting from the quantized folding of pDNA within polyplex micelles is promising for application in therapeutic gene delivery systems.

© 2011 Elsevier Ltd. All rights reserved.

1. Introduction

Development of safe and effective gene carriers is a key technology required for gene therapy. [1–5] A core issue for preparing non-viral gene carriers is the packaging of large pDNA molecules into the carrier system. Therefore, understanding the various packaging mechanisms is fundamental for the rational design and construction of gene carrier systems capable of achieving effective gene transfer. A key aspect of pDNA packaging is pDNA condensation. [6,7] DNA condensation is characterized as the large volume transition from a coil to a globule state, known as the coil–globule transition [8,9]. Until recently, the understanding of pDNA condensation has been mostly limited to morphological characterization of rod, toroid, and sphere structures [10,11] resulting from polyion complexation with polycations. Details pertaining to how and why pDNA is condensed into such structures and conditions required to selectively prepare these structures, as well as the effect of these packaging structure on gene expression remain to be fully clarified. This lack of understanding is mainly attributed to the difficulty of observing the condensation process of a single pDNA molecule, as condensation occurs concurrently with intercomplex aggregation particularly at charge-neutral ratios of polyions. To address this issue, block catiomers composed of a neutral hydrophilic poly(ethylene glycol) (PEG) segment and a cationic poly(L-lysine) (PLys) segment were used to induce controlled pDNA condensation into polymeric micelles, i.e., polyplex micelles. [12–15] In this approach pDNA is spontaneously condensed and packaged into a polyplex micelle core surrounded by PEG, eventually resulting in condensation of a single pDNA molecule without intercomplex aggregation. This allows for observation of the DNA condensation process even in the charge-neutral region. By using cationic block copolymers we have elucidated a highly regulated mechanism for pDNA condensation that involves folding into quantized-length rods. Rod lengths were found to be $1/2(n+1)$ of the original pDNA length by the folding of pDNA n times within polyplex micelles prepared with PEG-PLys 12–17 at the stoichiometric charge ratio (12 denotes the M_w of

* Corresponding author. Department of Materials Engineering, Graduate School of Engineering, The University of Tokyo, 7-3-1 Hongo, Bunkyo-ku, Tokyo 113-8656, Japan. Tel.: +81 3 5841 7138; fax: +81 3 5841 7139.
E-mail address: kataoka@bmw.t.u-tokyo.ac.jp (K. Kataoka).

0142-9612/$ – see front matter © 2011 Elsevier Ltd. All rights reserved.
doi:10.1016/j.biomaterials.2011.09.046

PEG in kDa, and 17 denotes Lys repeating units). [16] Furthermore, significantly higher gene expression efficiency was found in a cell-free transcription/translation system for pDNA packaged through the quantized folding within micelles compared to naked pDNA. Extension of this enhanced gene expression inherent to folded pDNA to living cells and ultimately whole organisms could greatly improve potential for therapeutic applications.

In this work, pDNA packaging within both rod and sphere shaped polyplex micelles was investigated, with a focus on DNA rigidity and folding. Selective preparation of rod or spherical structures was accomplished by modulating the PLys segment length of the block catiomer. Moreover, the correlation of these packaging structures to gene expression efficiency was determined both *in vitro* and *in vivo*, with improved gene expression resulting from folded pDNA demonstrated in cultured cells as well as in skeletal muscle following intravenous (IV) injection.

2. Materials and methods

2.1. Materials

A series of poly(ethylene glycol)-*b*-poly(L-lysine) (PEG-PLys) block copolymers with different PLys segment lengths were synthesized via ring-opening polymerization of N^{ε}–trifluoroacetyl-L-lysine *N*-carboxyanhydride initiated by the ω–NH_2 terminal group of α–methoxy-ω-amino PEG (M_w 12 k), followed by removal of trifluoroacetyl groups (TFA) by NaOH. The degree of polymerization (DP) of PLys segments were determined to be 20, 34, 38, 51, 70, and 88, respectively by comparing ^1H NMR integration ratios between PEG chain methylene protons (CH_2CH_2O) and of lysine unit methylene protons ($(CH_2)_3CH_2NH_3$). PEG-PLys block copolymers with various PLys chain lengths were denoted as 12–20, 12–34, 12–38, 12–51, 12–70, and 12–88, respectively. Gel permeation chromatography (GPC) measurements were carried out using a TOSOH HLC-8220. Molecular weight distributions (M_w/M_n) for all these block copolymers were determined to be less than 1.1.

Packaging studies primarily utilized pBR322 (4361 bp) pDNA, luciferase T7 control DNA (4315 bp) was used for cell-free transcription/translation assays, and EGFP encoding pDNA was used for cytoplasmic injection. pGL4-Luc was used for *in vivo* gene transfer studies. These pDNAs were amplified in competent DH5α *Escherichia coli* and then purified using a HiSpeed Plasmid MaxiKit purchased from QUIAGEN Science Co. Inc. (Germany). Texas Red labeled-dextran (M_w 70,000) was purchased from Molecular Probes (USA).

2.2. Methods

2.2.1. Formation of pDNA/PEG-PLys polyplex micelles

PEG-PLys block copolymer and pDNA were separately dissolved in 10 mM Tris–HCl buffer adjusted to pH 7.4. Polyion complexes between PEG-PLys and pDNA (polyplex micelles) were obtained by simply mixing both solutions at stoichiometric charge ratio of lysine units in PEG-PLys to nucleotide units in pDNA (N/P ratio = 1). The final pDNA concentration of the complexes was adjusted to 33.3 μg/ml.

2.2.2. AFM imaging

Atomic force microscopy (AFM) imaging was conducted using an MMAFM, Nanoscope IIIa (Veeco, USA) in tapping mode with standard silicon probes on a highly orientated pyrolytic graphite (HOPG) substrate. The obtained images were processed by flattening to remove the background slope of the substrate surface.

2.2.3. TEM observation

TEM observation was conducted using an H-7000 electron microscope (Hitachi, Tokyo, Japan) operated at 75 kV acceleration voltage. Copper TEM grids with carbon-coated collodion film were glow-discharged for 20 s using an Eiko IB-3 ion coater (Eiko Engineering Co. Ltd., Japan). The grids were dipped into complex solution, which was mixed with uranyl acetate (UA) solution (2% (w/v)), for 30 s. After excess solution was removed using a filter paper, the sample grids were allowed to dry in air.

2.2.4. S1 nuclease digestion

S1 nuclease digestion of complexes was carried out in 30 mM sodium acetate buffer (pH 4.6) containing 1 mM $ZnSO_4$ for 30 min at 37 °C. The nuclease concentration was 5 units relative to 1 μg of pDNA. The reaction was stopped by the addition of excess ethylenediamine tetraacetic acid (EDTA). Ten equivalents (relative to nucleotides) of sodium dextran sulfate (M_w 25,000) was added to the solution for 1 h to dissociate the complex, followed by gel electrophoresis to determine the fragment lengths through a 0.9% agarose gel in electrophoresis buffer (20 mM Tris-AcOH, 10 mM NaOAc, 0.5 mM EDTA, and pH 7.8).

2.2.5. Cell-free transcription/translation assay

Cell-free gene expression efficiency was evaluated using the TnT Quick Coupled Transcription/Translation System (Promega Co., USA) using luciferase T7 control DNA coding the luciferase gene. Luciferase expression was achieved by mixing solutions of naked pDNA or polyplex micelles, each containing 1.33 μg of pDNA, with the solution from the cell-free system (TnT T7 Quick Master Mix) and this mixture was incubated for 90 min at 37 °C according to the protocol provided by the manufacturer. Luciferase expression was evaluated following addition of luciferase substrate (Luciferase Assay Reagent, Promega Co., USA) using a Mithras LB 940 luminometer (Berthold Technologies, Germany).

2.2.6. DNase I activity towards complexed pDNA

Solution containing DNase I (0.01 units, 25 mM $MgCl_2$ in Tris–HCl buffer (pH 7.4)) was added to the complex solution (pBR322, 33.3 μg/ml) and incubated at 37 °C. After the intended time, an excess amount of EDTA was added to stop the enzymatic reaction. Next, an excess amount of dextran sulfate was added to dissociate the polyplex micelles. After 3 h of incubation the solution was subjected to gel electrophoresis. DNA bands corresponding to supercoiled (SC), open-circular (OC), and linear forms were taken as the remaining pDNA, as these forms contribute to the transcription. DNase activity towards pDNA was determined by the intensity sum of the SC, OC, and linear forms respect to the intensity of non-DNase treated bands (naked pDNA) using densitometry.

2.2.7. In vitro transcription efficiency

A solution containing all necessary elements for transcription, *i.e.*, 0.5 mM ribonucleotides mixture (ATP, CTP, GTP, and UTP (Promega Co., USA)), 5 mM $MgCl_2$, 100 mM NaCl, and 5 mM DTT in10 mM Tris–HCl (pH 7.4) was added to solution containing either naked pDNA or pDNA complexed with PEG-PLys. T7 RNA polymerase (Promega Co., USA) (30 units) was then added to this mixture, followed by further incubation for 2 h at 37 °C. The solution was then incubated at 95 °C for 10 min to deactivate RNA polymerase. Template pDNA was digested by 30 units of DNase I at 37 °C for 2 h. PEG-PLys was digested by adding trypsin-EDTA at 37 °C for 2 h. Next, the solution was mixed with Quant-iT RiboGreen RNA reagent (fluorescent dye for RNA quantitation) for 30 min in the dark. Quantification of transcribed mRNA was determined using a spectro-fluorometer (λ_{ex} = 365 nm, λ_{em} = 590 nm). The fluorescence intensity of the transcribed mRNA from the polyplex micelles was normalized to that of mRNA from the naked pDNA.

2.2.8. Cytoplasmic microinjection

pDNA encoding for EGFP was injected into the cytoplasm of Huh-7 cells (100 cells) either in the naked form or packaged within polyplex micelles using a Micromanipulator NI2 and Microinjector FemtoJet (Eppendorf, Germany). Injections were conducted using depth limitation, with the settings of P_i = 100 hPa, P_c = 30 hPa and 0.1 s injection time, via glass micropipettes. Texas Red-labeled dextran (M_w 70,000), a charge-neutral fluorescence dye, was co-injected to allow estimation of the total injection volume. After 24 h incubation at 37 °C, 5% CO_2, the fluorescence intensity of EGFP was measured by fluorescence microscopy. Gene expression was quantified using expressed EGFP fluorescence and Texas Red-dextran fluorescence as a standard with following equation:

$$\sum_{i=1}^{n}\left[\left(I_{green}-I_{back.green}\right)/t_{GFP}\right]\Big/\sum_{i=1}^{n}\left[\left(I_{red}-I_{back.red}\right)/t_{Texas-red}\right] \tag{1}$$

Here, I_{green} = fluorescence intensity of EGFP, $I_{back\,green}$ = fluorescence intensity of the background at the detection wavelength, I_{red} = fluorescence intensity of Texas Red-dextran, $I_{back\ red}$ = fluorescence intensity of the background at the detection wavelength, t_{GFP} or $t_{Texas\text{-}Red}$ = exposure time for EGFP or Texas Red, respectively. The value determined by the above equation yields gene expression activity per injected pDNA molecule.

2.2.9. In vivo gene transfer within skeletal muscle tissue

A solution containing naked pDNA or polyplex micelles (300 μL, 50 μg of luciferase-expressing pDNA) was injected into a distal site in the great saphenous vein of the mouse hind limb. A tourniquet was placed on the proximal thigh to transiently restrict blood flow prior to injection and remained in place until 5 min post-injection. Gene expression was determined 5 days post-injection by measuring bioluminescence with an IVIS™ Imaging System (Xenogen, USA). Images and measurements of bioluminescent signals were acquired and analyzed using Living Image software (Xenogen, USA). Ten minutes prior to *in vivo* imaging, the mice received the substrate D-luciferin (Biosynth, USA) at 150 mg/kg in PBS by intraperitoneal injection and were anesthetized using 1–3% isoflurane (Abbott Laboratories, USA). Animals were placed onto warmed (37 °C) stage inside the camera box and received continuous exposure to 1–2% isoflurane to sustain sedation during imaging. Luciferase expression was digitized and electronically displayed as a pseudocolor overlay onto a gray scale animal image. All animal experimental procedures were performed in accordance with the Guide for the Care and Use of Laboratory Animals as stated by the University of Tokyo.

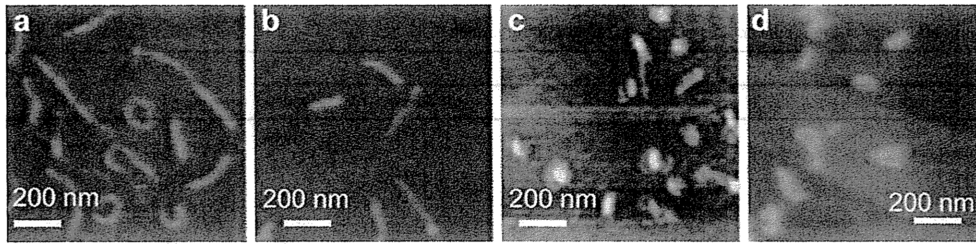

Fig. 1. AFM images of polyplex micelles. (a) 12–20, (b) 12–38, (c) 12–51, and (d) 12–70. All images were acquired in tapping mode.

3. Results and discussion

3.1. Packaging of pDNA within polyplex micelles

In order to further explore the packaging of pDNA within polyplex micelles, the structures of 12–20, 12–38, 12–51, and 12–70 polyplex micelles prepared at charge stoichiometric ratio were investigated using atomic force microscopy (AFM). Rod and toroid structures were observed for 12–20 and 12–38 polyplex micelles (Fig. 1a and b), similar to previously studied 12–17 based polyplex micelles. Careful analysis of 12–17 polyplex micelles revealed that rod structures formed as a result of the quantized folding of pDNA. [16] In contrast, spherical structures were obtained for 12–51 and 12–70 polyplex micelles (Fig. 1c and d). In the case of 12–20 and 12–38 polyplex micelles, precise rod lengths were measured from TEM images (representative TEM images are shown in Supporting Information 1) to determine whether or not rod structures follow the quantized folding model. It should be noted that TEM was performed with uranyl acetate (UA) staining, which allows selective observation of DNA due to the stronger affinity of UA to DNA compared to PEG. According to the quantized folding model (Fig. 2a), rod lengths are restricted to 1, 1/2, 1/3, 1/4 increments relative to the length of an unfolded rod structure (depicted in Fig. 2a structure (i)). Using the unfolded rod structure as a standard, which is calculated to be 611 nm for pBR322 (4361 bp) [16], the theoretical rod lengths are calculated to be 305, 203, 152, 122, 102, 87, and 76 nm by folding of pDNA 1, 2, 3, 4, 5, 6, and 7 times, respectively (Table 1). Note that estimation of the standard rod length (611 nm) involves, (1) simply collapsing the circular DNA results in half of the contour length (4361 (bp) $\times$ 0.338 (nm/bp)/2), (2) length reduction due to the coiled-coil form of pDNA caused by its inherent superhelicity, and (3) artifacts in TEM observation on a collodion substrate with UA staining [17]. These theoretical rod lengths (shown as dotted lines in Fig. 2b) correlate very well to

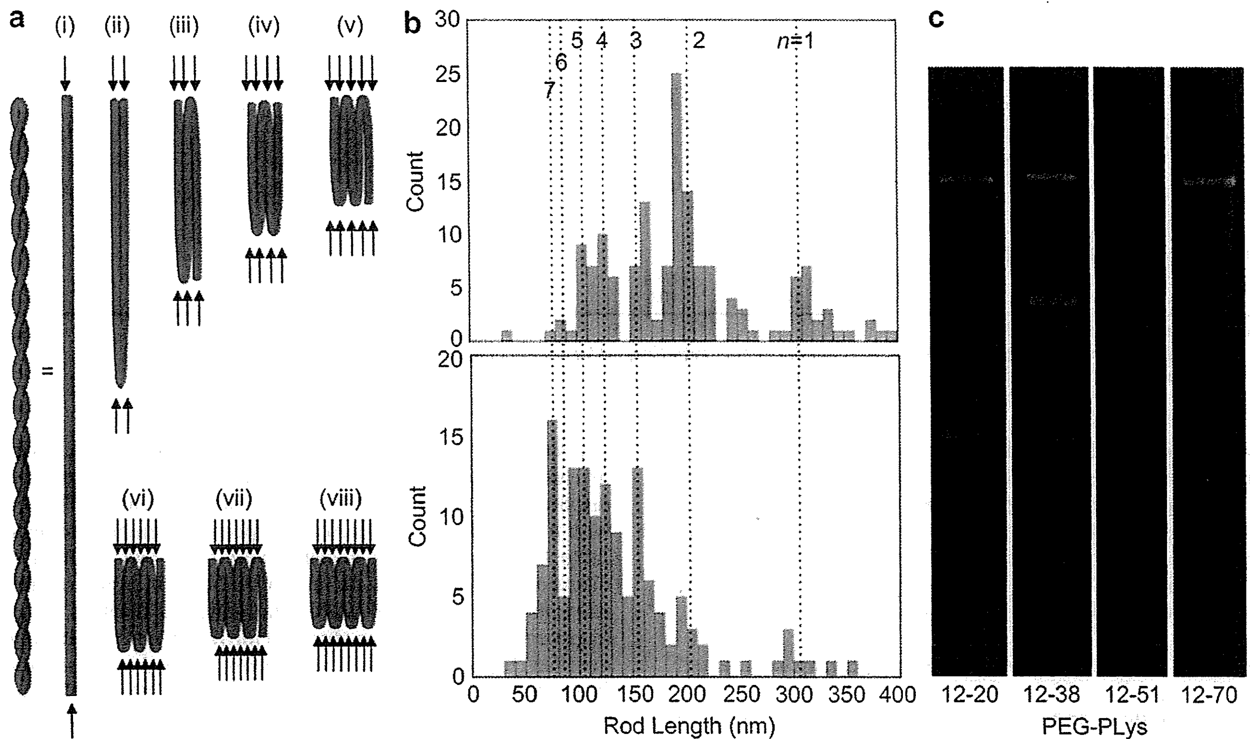

Fig. 2. Quantized folding of pDNA into polyplex micelles. (a) Schematic illustration of pDNA condensation into rod structures with quantized folding. The rod structure formed by simply collapsing supercoiled circular pDNA is depicted as (i). For simplification, intertwining due to superhelicity is not pictured. S1 nuclease-susceptible sites (sites of single-stranded DNA formed by dissociation of double-stranded DNA) are indicated by arrows. Note that the PEG shell is not pictured and that folded DNA strands are depicted in 2-dimentions for simplicity, however they are 3-dimensionally packed into bundles. (b) Distribution of the long axis length of the rod structures measured from TEM images for the polyplex micelles of 12–20 (top, 168 counts) and 12–38 (bottom, 141 counts). Dotted lines represent calculated rod lengths according to quantized folding. (c) S1 nuclease activity toward the polyplex micelles of 12–20, 12–38, 12–51 and 12-70 determined by gel electrophoresis.

Table 1
Expected fragment fractions and length of the rod structures in the quantized folding model.

Expected fregment fraction[a]								Fraction	Fragment No. in Table 2
$n = 0$	$n = 1$	$n = 2$	$n = 3$	$n = 4$	$n = 5$	$n = 6$	$n = 7$		
2/2	4/4	6/6	8/8	10/10	12/12	14/14	16/16	1.00	1
							15/16	0.94	
						13/14		0.93	
					11/12			0.92	
				9/10				0.90	
			7/8				14/16	0.88	
						12/14		0.86	
		5/6			10/12			0.83	2
							13/16	0.81	
				8/10				0.80	
						11/14		0.79	
	3/4		6/8		9/12		12/16	0.75	3
						10/14		0.71	
				7/10				0.70	
							11/16	0.69	
		4/6			8/12			0.67	4
						9/14		0.64	
			5/8				10/16	0.63	
				6/10				0.60	
					7/12			0.58	(5)[c]
						8/14		0.57	5
							9/16	0.56	(5)
1/2	2/4	3/6	4/8	5/10	6/12	7/14	8/16	0.50	6
							7/16	0.44	
						6/14		0.43	(7)
					5/12			0.42	7
				4/10				0.40	
			3/8				6/16	0.38	8
						5/14		0.36	
		2/6			4/12			0.33	9
							5/16	0.31	
				3/10				0.30	
						4/14		0.29	10
	1/4		2/8		3/12		4/16	0.25	11
						3/14		0.21	
				2/10				0.20	12
							3/16	0.19	(12)
		1/6			2/12			0.17	13
						2/14		0.14	14
			1/8				2/16	0.13	15
				1/10				0.10	
					1/12			0.08	
						1/14		0.07	
							1/16	0.06	
multiples and expected length[b] (nm)									
x/2	x/4	x/6	x/8	x/10	x/12	x/14	x/16		
611	306	204	153	122	102	87	76		

[a] Ratio respect to the original pDNA length.
[b] Expected rod length in TEM images considering shrinkages due to the supercoiling and use of collodion substrate with UA staining.
[c] Fragment number in brackets is candidate for the band in Table 2.

measured rod length distributions from TEM images, suggesting that the rod structures of 12–20 and 12–38 polyplex micelles were formed by quantized folding. As seen in Fig. 2b, the rod size distribution of 12–38 polyplex micelles was found to be shorter compared to 12–20 polyplex micelles. Note that no rod structures were observed for 12–51 and 12–70 polyplex micelles (Fig. 1c and d), thus rod length distribution was not measured.

3.2. Integrity of double-stranded DNA within polyplex micelles

We previously reported that rod structures are formed by folding rigid double-stranded DNA (persistence length (l_p) of approximately 50 nm [18]) at the rod ends via hairpin turns. This is made possible by dissociation of the double-stranded structure into more flexible single-strand species [19] with l_p of only a few nanometers [20] or less. [21] Double-strand dissociation sites, or fold sites, were detected by S1 nuclease digestion, as this nuclease is a single-strand specific cleavage enzyme. Enzymatic digestion revealed a characteristic fragmentation pattern with lengths corresponding to multiples of $1/2(n+1)$ of the original pDNA length, with n being the folding number (expected fragments are listed in Table 1). Thus, polyplex micelles were subjected to S1 nuclease digestion in this study to investigate the integrity of double-stranded DNA contained within the polyplex micelles. A distinct fragmentation pattern was obtained for 12–20 and 12–38 polyplex micelles (Fig. 2c). Analysis of fragments showed that the ratios of fragment length with respect to the original pDNA length (Table 2) corroborated well with expected fragment lengths (Table 1) assuming quantized folding of pDNA within 12–20 and 12–38 polyplex micelles. In contrast, the gel electrophoresis profiles for 12–51 and 12–70 polyplex micelles were smeared and faint (Fig. 2c). This suggests that dissociation and nuclease cleavage of the double-stranded DNA structure occurred randomly. Note that these polyplex micelles were observed to adopt irregular and

Table 2
Fragment lengths and fractions respect to the linearized pDNA length for pBR322 complexed by PEG-PLys block catiomers.

No.	Fragment length (bp)[a] and fractions[b]						Possible folding number
	PEG-PLys 12–20			PEG-PLys 12–38			
1	s[c]	4452	1	s	4458	1	0,1,2,3,4,5,6,7
2		3799	0.85	s	3712	0.83	2,5
3	s	3195	0.71	s	3328	0.75	1,3,5,7,
4	s	2943	0.66	s	2962	0.66	2,5
5		2555	0.57		2540	0.57	6 (or 5,7)[d]
6	s	2228	0.5	s	2223	0.5	0,1,2,3,4,5,6,7
7		1925	0.43		1885	0.42	5 (or 6)
8					1666	0.37	7
9		1482	0.33	s	1466	0.33	2,5
10		1263	0.28		1262	0.28	6 (or 4)
11	s	1063	0.24	s	1078	0.24	1,3,5,7
12		854	0.2		861	0.19	4 (or 7)
13		727	0.16	s	726	0.16	2,5
14		634	0.14				6
15					564	0.13	3,7

[a] Fragment length were estimated from size marker.
[b] Each fragment length was devided by the length of the linear band, *i.e.*, fragment no.1.
[c] s; band with strong fluorescence intensity.
[d] () possible folding number.

compact spherical structures in AFM images (Fig. 1c and d). Formation of such compact structures by the regular folding of rigid double-stranded DNA seems unlikely, considering the appreciably long l_p of ~50 nm for native double-stranded DNA [18] and the even longer l_p of ~90 nm for pDNA complexed with PEG-PLys (due to the formation of the intertwining coiled-coil structure). [16] Presumably, dissociation of the double-stranded DNA structure and exposure of S1 nuclease-susceptible single strands may occur randomly at many sites within these polyplex micelles, eventually leading to formation of collapsed structures as a result of flexible single-stranded DNA.

Both AFM and S1 nuclease digestion results suggest that there is a correlation between the micelle structure and the double-stranded structure of pDNA contained in the micelle core. It is likely that integrity of pDNA double-stranded structure, in other words rigidity of DNA, plays a crucial role in discriminating between packaging structures. DNA double-strand dissociation and subsequent folding or collapsing is influenced by the PLys segment length upon complexation with block catiomer. The critical PLys length that divides packaging structures into folded rods or collapsed spheres is located between 38 and 51 amino acid units. Studies devoted to providing further insight into the mechanisms involved in this critical phenomenon are currently underway in our lab, and results will be reported in the near future.

3.3. *Effect of pDNA packaging on in vitro gene expression*

As described in the preceding section, structures of polyplex micelles are modulated by the PLys segment length and are categorized into two groups; 1) quantized folding packaging (12–20 and 12–38 polyplex micelles) mediated by a highly regulated folding mechanism, and 2) collapsed packaging (12–51 and 12–70 polyplex micelles), possibly accompanied by random dissociation of double-stranded DNA structure. Here, we addressed the relationship between the structure of the polyplex micelles and their transfection efficiency. Although polyplex micelles were prepared in solution without NaCl for characterization studies in the preceding section, the obtained results are reasonably extended to physiological buffer conditions used in biological assays because there was no substantial difference in the size and shape between polyplex micelles prepared at 0 and 150 mM NaCl judging from dynamic light scattering (DLS) measurement and TEM observation (Figs. S1 and S2 of the Supporting Information).

We have previously reported that polyplex micelles containing quantized folded pDNA, prepared from PEG-PLys 12–17, exhibit higher gene expression efficiency than naked pDNA in the cell-free transcription/translation assay system for luciferase expression. [16] This motivated us to compare the gene transfection efficiency of pDNA contained in micelles with different packaging modes depending on PLys length of the block copolymer. As seen in Fig. 3a, regularly folded pDNA contained in the core of polyplex micelles prepared with 12–20 and 12–38 achieved significantly higher luciferase expression than naked pDNA in the cell-free system reconstructed from rabbit reticulocyte cell lysate. This is consistent with our previous results obtained for polyplex micelles prepared with 12–17, which also comprise regularly folded pDNA [16]. Luciferase expression decreased for the collapsed pDNA in 12–70 polyplex micelles compared to the regularly folded pDNA in 12–20 and 12–38 polyplex micelles. Naked pDNA had the lowest expression efficiency out of all the formulations tested, even lower than 12–70 polyplex micelles, but this is likely due to poor tolerability of naked pDNA against nuclease degradation in the cell lysate [16]. Indeed, increased resistance against DNase I degradation was confirmed for all of the polyplex micelles regardless of the packaging mode, whereas naked pDNA was promptly digested under the same conditions (Fig. 3b).

Then, transcription efficiency of pDNA in different packaging modes was examined separately from the translation process, in conditions without interference from lysate components including nuclease. In this experiment, a reconstructed solution containing all necessary transcription components, i.e., ribonucleotides and RNA polymerases, was used, and the results are shown in Fig. 3c. No appreciable difference in transcription activity between 12–20 and 12–38 polyplex micelles and naked pDNA was observed, which is consistent with the view that decreased gene expression efficiency of native pDNA in cell-free system was caused by nuclease degradation (Fig. 3a). Collapsed pDNA contained in 12–70 polyplex micelles showed significantly lower transcription activity than the regularly folded pDNA contained in 12–20 and 12–38 micelles. This corroborates well with the trend observed in the gene expression assay shown in Fig. 3a, and suggests that a difference in transcription activity between regularly folded and randomly collapsed pDNA ultimately determines the final efficiency of gene expression.

Transcription requires that transcription machinery must first access, and then slide along double-stranded DNA. Comparable transcription activity of native pDNA with regularly folded pDNA contained in 12–20 and 12–38 polyplex micelles suggests that these transcription processes may not be hindered by the block copolymers complexed with pDNA. Presumably, exchange of these block copolymers with transcription machinery may occur in the transcription processes for regularly folded pDNA with a well-preserved double-stranded structure. Another possibility is that polyplexes already dissociated in solution prior to transcription, but that is apparently not the case. As seen in Fig. 3b, pDNA in the 12–20 and 12–38 polyplex micelles showed appreciably higher resistance against nuclease digestion than native pDNA, indicating the polyplex stability in medium. Alternatively, the significantly lowered transcription activity of collapsed pDNA contained in 12–70 polyplex micelles indicates that transcription machinery is substantially impeded in this case. It is of interest to note that the S1 nuclease digestion study (Fig. 2c) demonstrated substantial and random disruption of the double-stranded DNA structure packaged in the 12–70 polyplex micelle. Thus, one plausible reason for transcription inhibition may be the inability of transcription machinery to slide along DNA strands. However, decreased